JOURNAL OF GEOPHYSICAL RESEARCH, VOL. 107, NO. A7, 1106, 10.1029/2000JA003501, 2002

Simultaneous observations of earthward flow bursts and plasmoid ejection during magnetospheric substorms

J. A. Slavin,[1] D. H. Fairfield,[1] R. P. Lepping,[1] M. Hesse,[1] A. Ieda,[1] E. Tanskanen,[2] N. Østgaard,[3] T. Mukai,[4] T. Nagai,[5] H. J. Singer,[6] and P. R. Sutcliffe[7]

Received 29 November 2000; revised 19 March 2001; accepted 19 March 2001; published 11 July 2002.

[1] Examination of observations taken by radially aligned International Solar Terrestrial Physics spacecraft in the nightside magnetosphere on 9 July 1997 has revealed close temporal correlations between earthward flow bursts in the plasma sheet and the ejection of plasmoids. A one-dimensional model of plasma sheet flow is applied to these observations to determine the time and location for the initiation of lobe flux tube reconnection. For the single clear flow burst-plasmoid pair observed during the first substorm and the three pairs produced by the second substorm, lobe flux reconnection was inferred to have started at $X \sim -15$ to -18 R_E, respectively, about 2–5 min prior to the observations of substorm expansion phase onset. These time delays and propagation speeds are shown to be consistent with the measured plasma sheet bulk flow speeds. Substorm expansion phase onset was essentially coincident with the arrival of the flow bursts at Geotail, which was located near the inner edge of the plasma sheet at $X \sim -9$ R_E. The dipolarization of the magnetic field at geosynchronous orbit, auroral kilometric radiation (AKR) emissions, Pi2 pulsations, high-latitude negative magnetic bays, and auroral breakup marking substorm expansion onset are all coincident within the ±1 min resolution of the measurements. Accordingly, it appears that earthward of the inner edge of the plasma sheet, where Geotail was located, substorm effects propagated at speeds comparable to the Alfven speed characteristic of the high-latitude inner magnetosphere, $\sim 10^3$ km s^{-1}. In summary, the results of our investigation strongly support the modern near-Earth neutral line (NENL) model of substorms in which the onset of lobe flux tube reconnection in the near tail is followed ~2–5 min later by the braking of earthward flow bursts as they encounter the inner magnetosphere and within ~1 min, by Pi2s generations, current wedge development, and AKR and auroral expansion, and finally, ~10–20 min later, by the tailward retreat of the neutral line and either the development of a new NENL or the initiation of the recovery phase. *INDEX TERMS:* 2788 Magnetospheric Physics: Storms and substorms; 2744 Magnetospheric Physics: Magnetotail; 2407 Ionosphere: Auroral ionosphere (2704)

1. Introduction

[2] Magnetospheric substorms are defined as intervals of intense energy dissipation lasting from about 30 min to several hours during which a reproducible pattern of auroral variations are present at high latitudes [*Akasofu*, 1964]. The beginning of the substorm is typically preceded by a "growth phase" lasting from tens of minutes to perhaps an hour [*McPherron et al.*, 1973] during which energy is accumulated in the magnetic fields of the tail lobes and growth occurs in the area of the polar cap as the quite time auroral oval moves to lower latitudes. Energy is dissipated in the ionosphere and inner magnetosphere and lost to flow down the tail during the "expansion phase" so named for the poleward expansion of the auroral oval as the magnetic fields in the tail lobes reconnect to power the substorm. The "onset" of the expansion phase is marked not only by the "breakup" of the preexisting quiescent auroral oval, but also the strengthening of westward electrical currents in the ionosphere near midnight, enhanced auroral kilometric radiation (AKR) emissions emanating from the auroral electron acceleration regions above the discrete auroral arcs, and the arrival of Pi2 pulsations at midlatitudes. Operationally, the earliest time when any of these phenomena are observed is often taken to be the onset of the substorm, but the confidence in the determination of when a substorm begins is greatest when the temporal discrepancies between these expansion phase onset indicators are small. Fortunately, the most common temporal dispersion among these onset signals is only a few minutes [*Slavin et al.*, 1993; *Liou et al.*, 1999, 2000a, 2000b; *Kepko and Kivelson*, 1999; *Kepko et al.*, 2001]. The duration of the expansion phase is quite variable but is typically 30 min to 2 hours for isolated substorms [e.g., *Craven and Frank*, 1991]. The substorm ends with a gradual reduction in the rate of energy dissipation in all regions of the ionosphere-magnetosphere system. This "recovery" phase is perhaps the least well defined and understood [*McPherron*, 1991].

[3] The temporal and spatial evolution of magnetospheric substorms is an important and enduring problem in space plasma physics. Its solution will entail a mature understanding of where and when these events begin, how and from where they draw their energy, and the manner in which this energy is transferred and dissipated throughout geospace. At this time only the near-Earth neutral line (NENL) model of substorms [*McPherron et al.*, 1973;

[1]Laboratory for Extraterrestrial Physics, NASA/Goddard Space Flight Center, Greenbelt, Maryland, USA.
[2]Geophysics Division, Finnish Meteorological Institute, Helsinki, Finland.
[3]Space Sciences Laboratory, University of California, Berkeley, California, USA.
[4]Institute of Space and Astronautical Science, Kanagawa, Japan.
[5]Department of Earth and Planetary Sciences, Tokyo Institute of Technology, Tokyo, Japan.
[6]NOAA Space Environment Center, Boulder, Colorado, USA.
[7]Hermanus Magnetic Observatory, Hermanus, South Africa.

Copyright 2002 by the American Geophysical Union.
0148-0227/02/2000JA003501$09.00

Baker et al., 1996] is sufficiently well developed to make self-consistent non–ad hoc predictions regarding how substorm effects rapidly appear throughout the magnetosphere in a reproducible and coherent fashion. This model forms the basis for our rapidly maturing ability to simulate magnetospheric substorms using MHD [*Lyon et al.*, 1998; *Ogino and Walker*, 1998; *Birn et al.*, 1999; *Raeder et al.*, 2000] and kinetic [*Shay et al.*, 1998; *Hesse et al.*, 1999; *Kuznetsova and Hesse*, 2000] numerical codes. At this time the only competing concepts focus on local instabilities or events in the inner magnetosphere [*Lui*, 1996; *Rostoker*, 1996; *Erickson et al.*, 2000] that might precede and trigger the onset of reconnection in the tail and its associated energy release.

[4] Tail reconnection must begin late in the substorm growth phase and initially involve only closed magnetic flux tubes in the relatively dense central plasma sheet where the Alfven speed is only $\sim 10^2$ km s^{-1} [*Hones*, 1977; *Taguchi et al.*, 1998]. This is a necessary precursor to lobe flux tube reconnection because the preexisting plasma sheet must be removed in order to bring the two lobes together. The magnetic fields in the plasma sheet are weak in the sense that this is a high-β region and only modest amounts of magnetic energy are available to be converted into particle energy. Because of the low Alfven speed, the rate of reconnection in the tail is thought to proceed very slowly initially, when only plasma sheet flux tubes are involved, and then grow "explosively" when lobe flux tubes with their Alfven speeds of a thousands km s^{-1} or more begin to reconnect [e.g., *Hesse et al.*, 1996].

[5] Reconnection alters the stress balance of the plasma sheet by "disconnecting" much of the downstream plasma sheet from the Earth. The high-speed flow out of the neutral line leads to the ejection of the downstream plasma sheet at high speed, typically $\sim$300–800 km s^{-1}, in the form of a "plasmoid" [*Hones*, 1977; *Ieda et al.*, 1998; *Haland et al.*, 1999a]. Observationally, plasmoids are known to occur singlely, in pairs, or groups of three or more with nearly equal probability [*Slavin et al.*, 1993; *Ieda et al.*, 1998]. How the reconnection in the near tail leads to the formation and ejection of multiple plasmoids in rapid succession during the span of a single substorm remains to be explained [*Jin et al.*, 2001].

[6] The dynamics of the near-Earth plasma sheet has proven to be even more complex than those of the deep tail with the transport of magnetic flux and plasma and the generation of field-aligned currents closing in the ionosphere all linked at a fundamental level [e.g., *Atkinson*, 2000]. Geotail observations have shown on a statistical basis that the NENL typically forms several minutes prior to substorm onset typically at distances of $X \sim -20$ to -30 R_E, preferentially in the premidnight region of the tail [*Nagai et al.*, 1998; *Machida et al.*, 1999; *Baumjohann et al.*, 1999]. The high-speed earthward flows produced by the reconnection are "bursty" on timescales of $\sim$1–10 min [*Baumjohann et al.*, 1990; *Angelopoulos et al.*, 1994], and they have peak speeds from several hundred km s^{-1} to over 1000 km s^{-1} [*Nagai et al.*, 1998; *Fairfield et al.*, 1998; *Machida et al.*, 1999]. *Angelopoulos et al.* [1992] has termed these short-duration, fast earthward flows bursty bulk flows (BBFs) and shown that they appear to carry enough northward B_z to complete *Dungey*'s [1961] magnetospheric magnetic flux transfer cycle.

[7] Studies examining BBFs have not always found a clear one-to-one correlation between substorm onsets and BBFs in the near tail in contrast to the high degree of correlation seen in the distant tail between plasmoids and substorms [*Slavin et al.*, 1992; *Moldwin and Hughes*, 1993; *Nagai et al.*, 1994]. These studies are complicated because of the difficulty in obtaining direct measurements of the near-Earth plasma sheet around substorm onset when the plasma sheet is known to thin dramatically, at times to less than an Earth radii [*McPherron and Manka*, 1985; *Fairfield*, 1988]. Similarly, *Ieda et al.* [2000] have conducted a statistical study indicating that Geotail sees many more plasmoids than earthward flow bursts. The most probable reason is the relatively small cross section of BBFs in the *Y-Z* plane, less than several R_E^2 [*Angelopoulos et al.*, 1996] versus plasmoids, $\sim$10–100 R_E^2 [e.g., *Slavin et al.*, 1999].

[8] In recent years, attention has also been given over to the interaction of the fast earthward flows with the inner magnetosphere. In particular, it has been shown that these earthward flows must slow as they "ram" into the stronger, more dipolar magnetic flux tubes found closer to the Earth and that the "braking" process will drive strong field-aligned currents [*Hesse and Birn*, 1991; *Shiokawa et al.*, 1997; *Birn et al.*, 1999]. Furthermore, the strength and direction of these currents are consistent with those required to form the substorm current wedge (SCW) [*Hesse and Birn*, 1991; *Birn et al.*, 1999]. A significant fraction of the cross-tail current in the near tail is known [*McPherron et al.*, 1973] to be diverted via field-aligned currents (FACs) down into the dawnward side of the midnight sector of the auroral oval at substorm onset, where it adds to the westward electrojet [*Kamide and Kokubun*, 1996], and then returns to the tail via outward FACs on the duskward side to form the SCW. Within the SCW the magnetic field moves toward a more dipolar configuration marked primarily by an enhanced northward magnetic field component or inclination. The manner in which the SCW initially forms and spreads longitudinally [*Kokubun and McPherron*, 1981; *Nagai*, 1982; *Singer et al.*, 1985] and radially down the tail [*Jacquey et al.*, 1991; *Slavin et al.*, 1997; *Ohtani et al.*, 1999] is still the subject of active research and sometimes conflicting results [e.g., *Hesse and Birn*, 1991; *Lui*, 1996; *Rostoker*, 1996].

[9] Early on 9 July 1997, while Wind and Polar were providing continuos solar wind and auroral observations, the IMP 8, Geotail, and GOES 8/9 satellites were nearly radially aligned in the magnetotail as shown in Figure 1. Together, these observations are unusual in that they provide near-simulataneous coverage of both the near and deep tail during two substorms whose expansion phases commenced at 0400 and 0602 UT, respectively, on this day. Combined with Canadian Auroral Network for the Open program Unified Study (CANOPUS) magnetic field measurements and ground-based Pi2 observations from the Hermanus Magnetic Observatory, this data set offers a rare opportunity to trace the temporal and spatial evolution of substorms in a common premidnight meridian from its origins in the upstream interplanetary medium, to the tail, to the inner magnetosphere, and finally, to the auroral ionosphere. Our analysis provides new insights into the causal relationship between earthward flow bursts in the plasma sheet and plasmoid ejection, including a new method for the determination of the time and location of open flux tube reconnection, and it lends quantitative support for the sequence of magnetospheric events predicted by the NENL model. In this manner our study adds to the growing body of knowledge of large-scale substorm dynamics being derived from the International Solar Terrestrial Physics (ISTP) mission [e.g., *Petrukovich et al.*, 1998; *Fairfield et al.*, 1998, 1999; *Slavin et al.*, 1999; *Haland et al.*, 1999a, 1999b; *Ohtani et al.*, 1999; *Sergeev et al.*, 2000; *Nagai et al.*, 2000; *Machida et al.*, 2000].

2. Event Selection

[10] In order to study the temporal and spatial evolution of magnetospheric substorms we desired to have as nearly as possible a radial alignment of spacecraft from geosynchronous orbit (SCW formation), to the near tail (earthward flow bursts) and the deep tail (plasmoid ejection) during a period of time when observations of the upstream solar wind and the auroral oval were available. These stringent requirements limited us to the period following the spring of 1996 by which time the apogee of the Geotail spacecraft had been lowered to 30 R_E and auroral images from the Polar spacecraft became routinely available. Accordingly, we elected to use GOES and Geotail as sources of measurements in the inner magnetosphere and near-tail, respectively, and IMP 8 for the detection of plasmoid ejection in the deep tail.

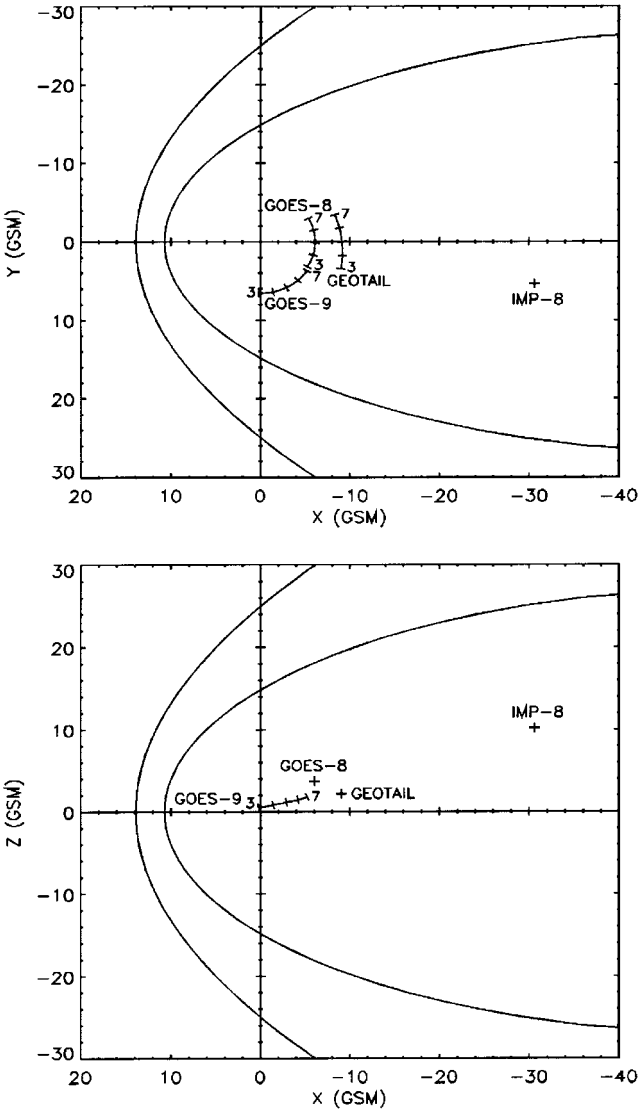

Figure 1. Trajectory plots for GOES 8 and 9, Geotail, and IMP 8 0300–0700 UT on 9 July 1997 in GSE coordinates.

[11] IMP 8's high inclination orbit and lack of a currently functioning plasma analyzer make it a poor source of direct plasmoid measurements. However, previous studies have shown that in 10–20% of substorms, plasmoid release can be detected at IMP 8 in the form a of a traveling compression region signature [*Moldwin and Hughes*, 1992; *Taguchi et al.*, 1997]. This modest detection probability is believed to be associated with instances when the NENL forms somewhat closer to the Earth than usual, giving the plasmoids additional time to grow and develop their characteristic north-south bulge that compresses the lobes to produce the traveling compression region (TCR) perturbation [*Taguchi et al.*, 1997, 1998]. Accordingly, 16 months of IMP 8 observations, June 1996 to October 1997, were searched for traveling compression region signatures, and a total of 43 such events were identified.

[12] Next, the Geotail database was searched to determine if this spacecraft had been located in the pre-midnight or midnight region of the near tail, i.e., $X > -15\ R_E$, during any of the IMP 8 plasmoid events. Furthermore, the Geotail-IMP 8 separation in GSM Y was specified to be <10 R_E. This requirement was levied to restrict the selection to situations where Geotail was properly positioned in local time to observe the earthward flow from the NENL that should accompany the tailward ejection of the plasmoid detected at IMP 8. In this manner it was hoped that both the earthward and tailward effects of reconnection at the NENL would be simultaneously observed. These requirements were strictly satisfied for only two of the IMP 8 events. As will be detailed in later sections, they were associated with two substorms that occurred early on 9 July 1997. IMP 8 and Geotail, as depicted Figure 1, were located in the midnight sector favored for substorm expansion phase onset in the auroral oval [*Craven and Frank*, 1991] and the observation of reconnection-driven fast flows in the plasma sheet [*Nagai et al.*, 1998, 2000; *Ieda et al.*, 1998, 2000]. The separations between these two spacecraft in GSM X and Y were 21.5 and 3.7 R_E and 21.3 and 7.0 R_E, respectively, for the first and second substorms.

3. July 9, 1997, Substorms

[13] Prior to the substorms investigated here the IMF, as measured by Wind, had been southward and variable for several hours, and the auroral zone was quite active. Other substorms occurred both before and after the 0300–0700 period that we will consider here. However, Geotail observations were not available between 2342 on 8 July and 0346 on 9 July and Geotail moved far into the dawn sector after our second substorm. Figure 2 shows the north-south component of the IMF in GSM coordinates, solar wind speed, density and dynamic pressure, the epsilon magnetospheric energy input parameter [*Perreault and Akasofu*, 1978], and the total lobe magnetic field intensity observed at IMP 8. The solar wind dynamic pressure was relatively constant over this period of time with the exception of a ~30% increase around 0520 UT at Wind. As Wind was located ~91 R_E upstream of IMP 8, the time delay for the propagation of this pressure change would have been $\sim 91 R_E/370$ km s^{-1} = 26 min (i.e., arrival at IMP 8 is ~0546). As expected, there is a small increase in the lobe field around this time with, B magnitude increasingly by a factor of $(P_D)^{1/2} = (1.3)^{1/2} = 1.14$ or ~1 nT. Otherwise, the Wind measurements suggest that the tail should be free from changes driven by varying external pressure.

[14] The epsilon parameter was quite variable, but it lay mostly between 100 and 200 GW, with the exception of a 20 min interval of northward IMF between ~0335 and 0355. As substorms are known to dissipate typically 10^{14-15} J [*Weiss et al.*, 1992; *Kallio et al.*, 2000], the expectation would be that the magnetospheric energy input predicted by epsilon would lead to a substorm every 10^3–10^4 (i.e., 15 min to 3 hours) on this day. Indeed, the Polar Ultraviolet Imager (UVI) auroral observations, which will be discussed in section 4, show two 30–60 min long increases in auroral emission intensity separated by ~90 min of relative quiescence. The correlated increases in auroral emission levels and poleward expansion identify these events as substorms beginning near 0400 and 0602. In each case the auroral intensity increases and expands poleward in the well-known substorm pattern [*Craven and Frank*, 1991]. As an aside, we note that the relative timing between the northward turning of the IMF, which causes the dropout in epsilon, and the onset of the first substorm is consistent with the former "triggering" the latter. For the second substorm, however, no obvious trigger was evident.

[15] The expansion, and then contraction, of the auroral oval can be seen more clearly in the next to bottom panel of Figure 2, where the area of the polar cap derived from the UVI measurements as a function of time is displayed. The uncertainty in this determination of polar cap area is estimated to be $\sim\pm 1 \times 10^6$ km^2 (M. Brittnacher, personnel communication, 2000). The expansion and contraction of the auroral oval is generally well correlated with the variation in auroral emission intensity and the strength of the lobe magnetic field observed at IMP 8. For the first substorm some decrease in polar cap area is suggested just prior to the first auroral onset and poleward expansion, but this variation is small and below the limit

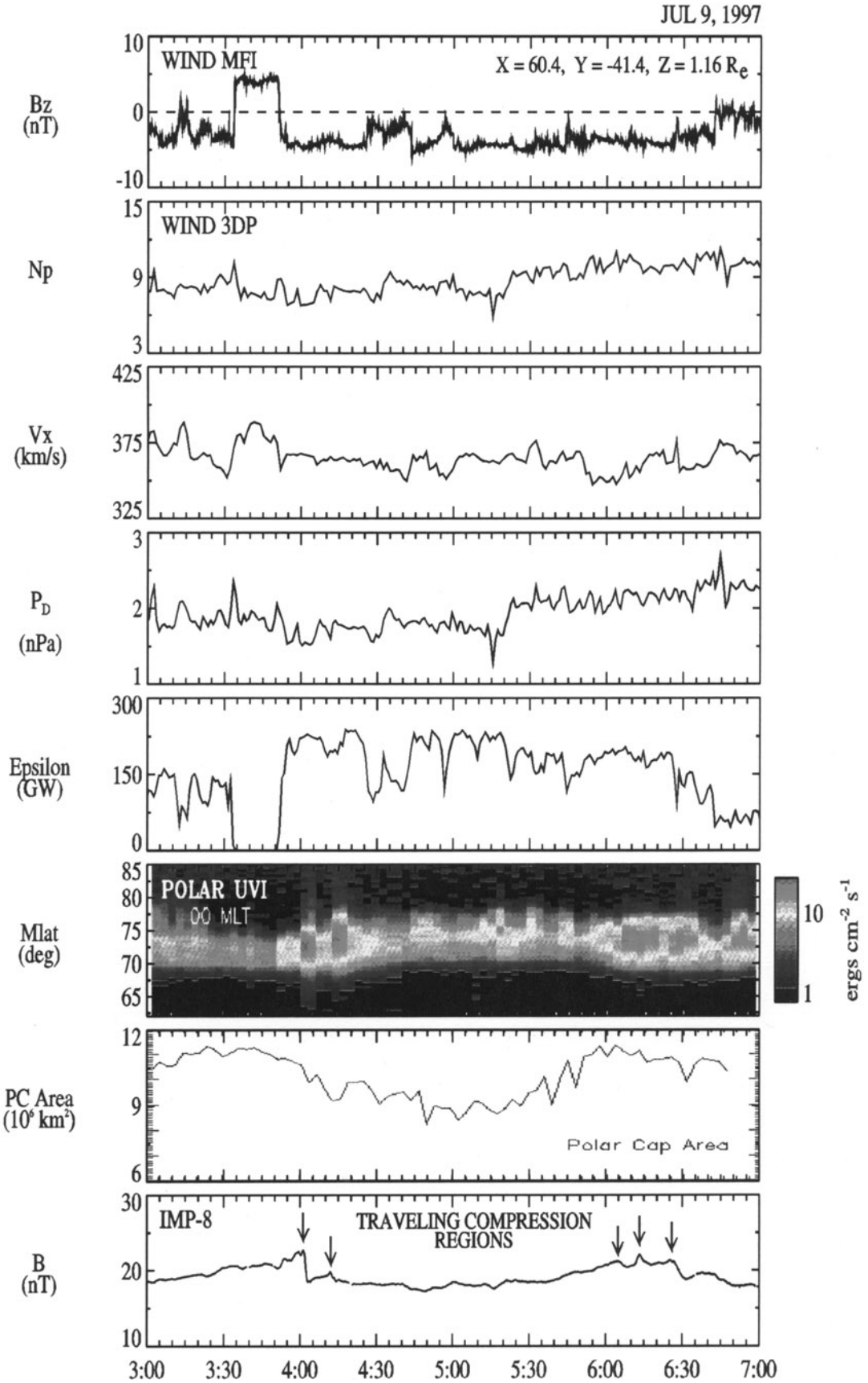

Figure 2. Solar wind and interplanetary magnetic field measurements upstream of the magnetosphere. A midnight sector auroral keogram and polar cap area from the Polar satellite and a plot of the lobe magnetic field intensity at IMP 8. The traveling compression regions are indicated with arrows. See color version of this figure at back of this issue.

of the uncertainty in the area determination. After the onset a rapid decrease in polar cap area is observed, which does not end until ~0500. The decrease in polar cap area for the second substorm begins promptly around the time when the emission intensity increases, but it proceeds more slowly than for the first substorm.

[16] The magnetic field at IMP 8 is observed to increase steadily between 0300–0400 and 0550–0605 as the lobes load with energy during the growth phase each substorm [*McPherron et al.*, 1973]. As just remarked, there is good correlation between the strength of the lobe magnetic field at IMP 8 and the polar cap area as would be expected from the basic principles of magnetic flux conservation and tail flaring [e.g., *Slavin et al.*, 1983]. The growth phases for both substorms with respect to lobe field strength and polar cap area are similar in duration, ~30 min, and their amplitudes, ~17–22 nT and ~8–11 × 10^6 km^2, respectively. Substorm expansion, characterized by auroral oval contraction and the lobe field magnitude decrease, takes place over an interval of ~30–45 min in both cases, but the contraction in oval area measured by UVI is less pronounced for the second substorm. However, in most cases where sharp drops in lobe field strength are recorded, for example, just after 0400 and around 0630, there are corresponding decreases in polar cap area. In between the substorms a broad minimum in the oval area and the lobe field intensity of ~8.5 × 10^6 km^2 and ~17.5 nT is present. Hence the full amplitude of the variations measured during these two substorms were factors of ~29 and 20% in polar cap area and lobe field strength, respectively. Ignoring the changes in tail flaring as its magnetic flux varies, a lower limit on the change in tail lobe magnetic energy content of ~44% can be estimated from the measured amplitude in the square of the magnetic filed strength.

[17] Finally, the two sets of TCRs, which led to the selection of these substorms for examination, are marked in Figure 2. TCRs are indicative of the onset of reconnection and the ejection of plasmoids and hence are typically observed just before and during the unloading of the tail lobes [*Slavin et al.*, 1993]. During the first substorm there is a close correlation between the two giant auroral breakups or poleward expansions seen in the UVI keogram and the two TCRs at IMP 8. For the second substorm, on the other hand, the auroral expansion is less structured, but longer in duration, and is accompanied by three TCRs.

4. Ionosphere: Auroral Emissions

[18] Polar UVI auroral measurements for 0300–0700 are displayed as keograms in Figure 3 [e.g., *Fillingim et al.*, 2000]. In the different local time panels, for each 1 hour of magnetic local time in width the intensity of the auroral ultraviolet emissions is displayed as a function of magnetic latitude. Only Lyman-Birge-Hopfield (LBH) long measurements were used in the creation of the keogram to avoid aliasing by mixing the images taken at two different wavelengths. The keogram resolution is limited to 3 min because the instrument was alternating images at the LBH short (140–160 nm) and LBH long (160–180 nm) wavelengths on this day [see *Torr et al.*, 1995]. The integration time for the images are 36.8 s with a new LBH long image every 3 min and 4 s. The use of this mode where the two filters alternate frequently limits the temporal resolution of the UVI images for the purposes of assessing substorm onset to several minutes [see *Liou et al.*, 2000a, 2000b].

[19] Between ~0300 and 0400 the auroral oval is evident, but rather dim, except near dawn, as it gradually expands toward lower magnetic latitudes. For several minutes prior to 0400 there is brightening at some local times, but no poleward expansion is seen. Beginning at 0400, the aurora in the 2100–0100 LT sector brightens strongly, i.e., the preexisting oval "breaks up," and rapidly expands poleward. This is the beginning of the classical auroral substorm expansion phase [e.g., *Craven and Frank*, 1991]. While the auroral oval continues to contract poleward, there is another sudden brightening and poleward leap at 0424. The aurora then ceases to contract and "recovers" to a well-defined oval with its poleward edge near ~77° magnetic latitude in the midnight sector. A second substorm then begins just after 0600. Again, some auroral brightening is apparent near midnight beginning several minutes earlier but without any poleward expansion. As with the first substorm, the poleward expansion in the midnight region is quite rapid and coincides with strong auroral brightening. After about 40 min the aurora starts to recover with the auroral oval again ~75–78 near midnight. In sections 5–9 we will examine other types of ionospheric and magnetospheric observations in order to track the initiation and development of these two substorms.

5. Inner Magnetosphere: Magnetic Dipolarization

[20] GOES 8 and 9 magnetic field measurements for the two July 9, 1997, substorms are displayed in Figure 4. H_p is directed parallel to the Earth's spin axis, H_e is radial toward the center of the Earth, and H_n is positive eastward. For the first substorm there are no clear signatures at GOES 9, which was near the dusk terminator. GOES 8 however, was in the premidnight sector where the substorm auroral bulge most frequently forms in the ionosphere at substorm onset and earthward flow bursts are found in the near-earth plasma sheet [e.g., *Fairfield et al.*, 1998, 1999]. At GOES 8 the magnetic field is observed to become more tail-like after ~0300 mirroring the lobe field loading observed farther down the tail at IMP 8. However, between 0330 and 0355 the field at GOES 8 contains a significant eastward deflection. This eastward deflection is the signature of either the intensification or the approach of field-aligned currents probably associated with the substorm growth phase [*Russell et al.*, 1994]. A few minutes later, at 0401:03, the first of two dipolarizations are observed in the H_p and H_e components with the magnetic field stepping to a more dipolar orientation.

[21] The second substorm is very similar to the first. It was preceded by 30–40 min of pronounced field line stretching at geosynchronous orbit, this time observed by GOES 9 (see spacecraft locations in Figure 1). This growth phase is, again, well correlated with the tail lobe loading seen in the IMP 8 magnetic field measurements at $X \sim -30\ R_E$. This time, there is little deflection in the east-west magnetic field component until just a few minutes prior to the dipolarization, and the field-aligned current signatures are weak. There is a single, sharp dipolarization of the GOES 9 magnetic field at 0601:40. Afterward the magnetic field is relatively steady except for a brief intensification of the cross-tail current or a close approach to this current layer around 0633 visible in the downward spike in B_p.

6. Near Tail: Earthward Flow Bursts

[22] The Geotail magnetic field and plasma measurements [*Mukai et al.*, 1994] for both substorms are shown in Figure 5 along with the Polar UVI keogram for midnight and the IMP 8 lobe magnetic field intensity. Vertical dashed lines mark the presence of earthward flow bursts in the Geotail plasma measurements. These flow bursts are well correlated with the two substorms and the traveling compression regions detected at IMP 8. The initial flow burst is associated with the first substorm, and the three later earthward flow bursts correspond to the onset and subsequent intensifications of the second substorm. In each case an earthward flow burst is paired with a tailward moving plasmoid (i.e., TCR). Only the second TCR during the first substorm lacks a clear earthward flow signature, albeit there is some enhanced variance in V_x. The existence of these correlated earthward/tailward moving plasmas is perhaps the most basic prediction of the NENL model of substorms; it will be the subject of additional analysis in later sections.

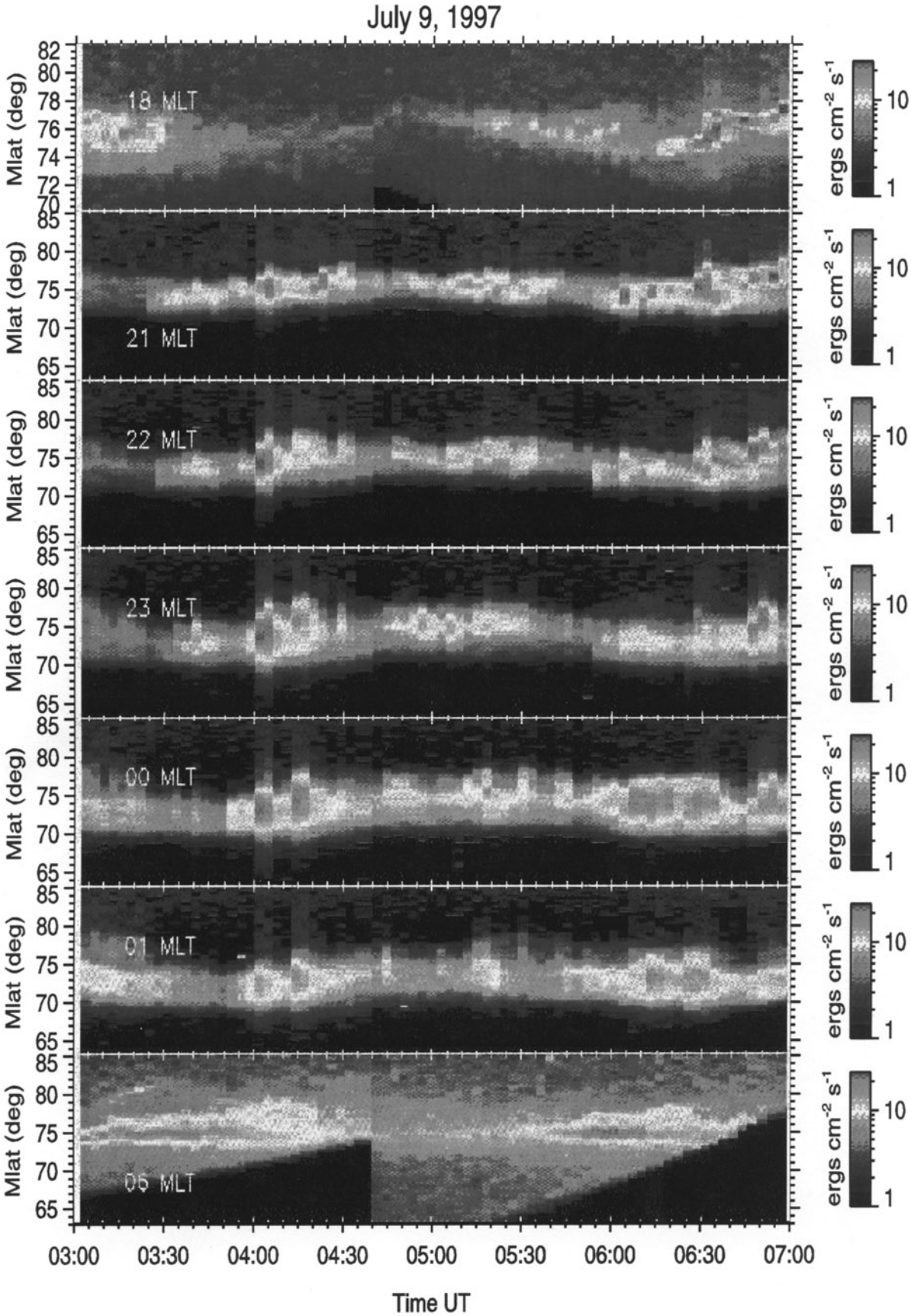

Figure 3. Auroral keograms (i.e., intensity as a function of latitude and universal time) with a spatial resolution of 1 hour in local time and 3 min in universal time. See color version of this figure at back of this issue.

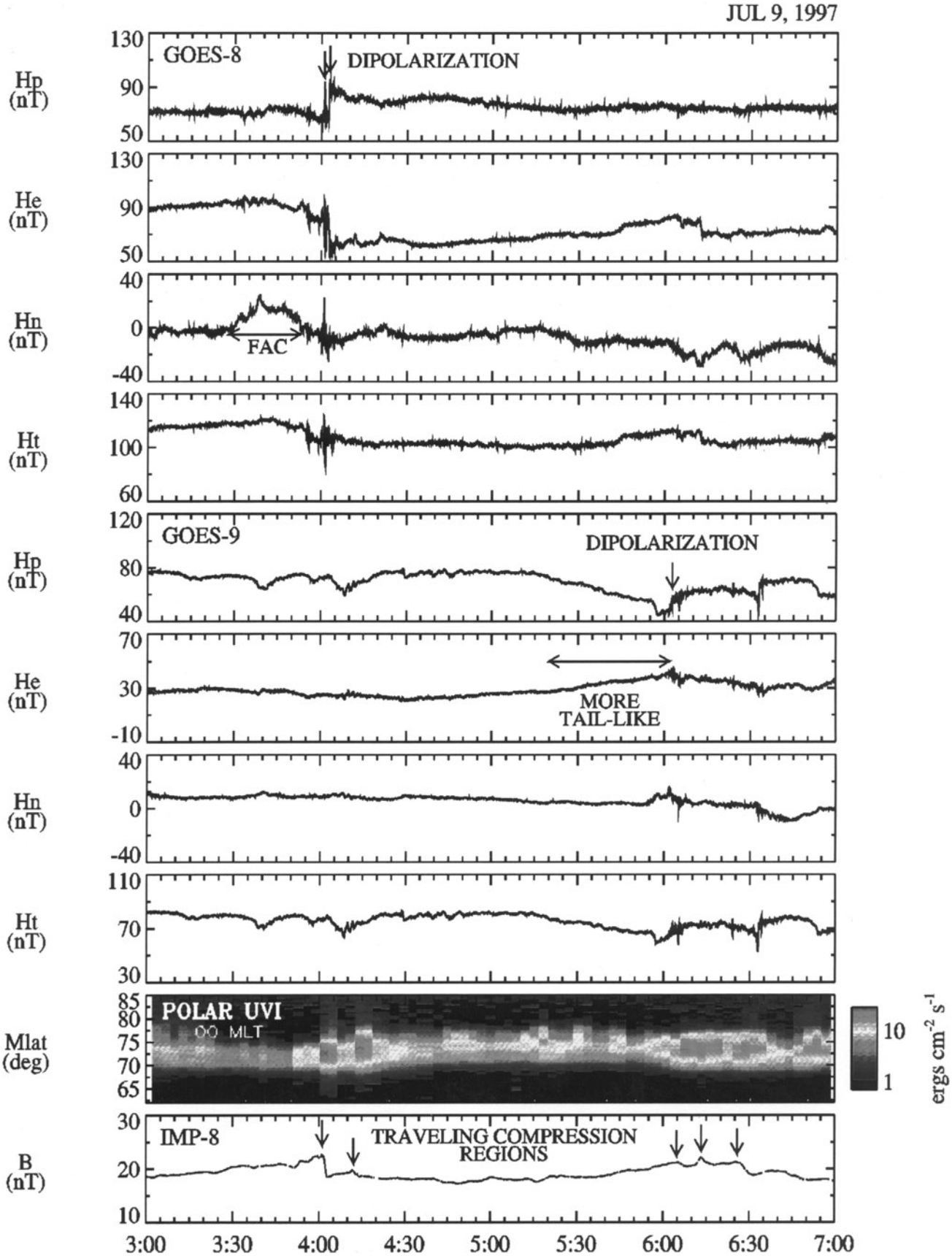

Figure 4. GOES 8 and 9 magnetic field observations in the coordinate system where H_p is parallel and opposite to the geomagnetic dipole, H_e is orthogonal to H_p and positive outward from the Earth, and H_n in positive eastward and completes the right-handed system. See color version of this figure at back of this issue.

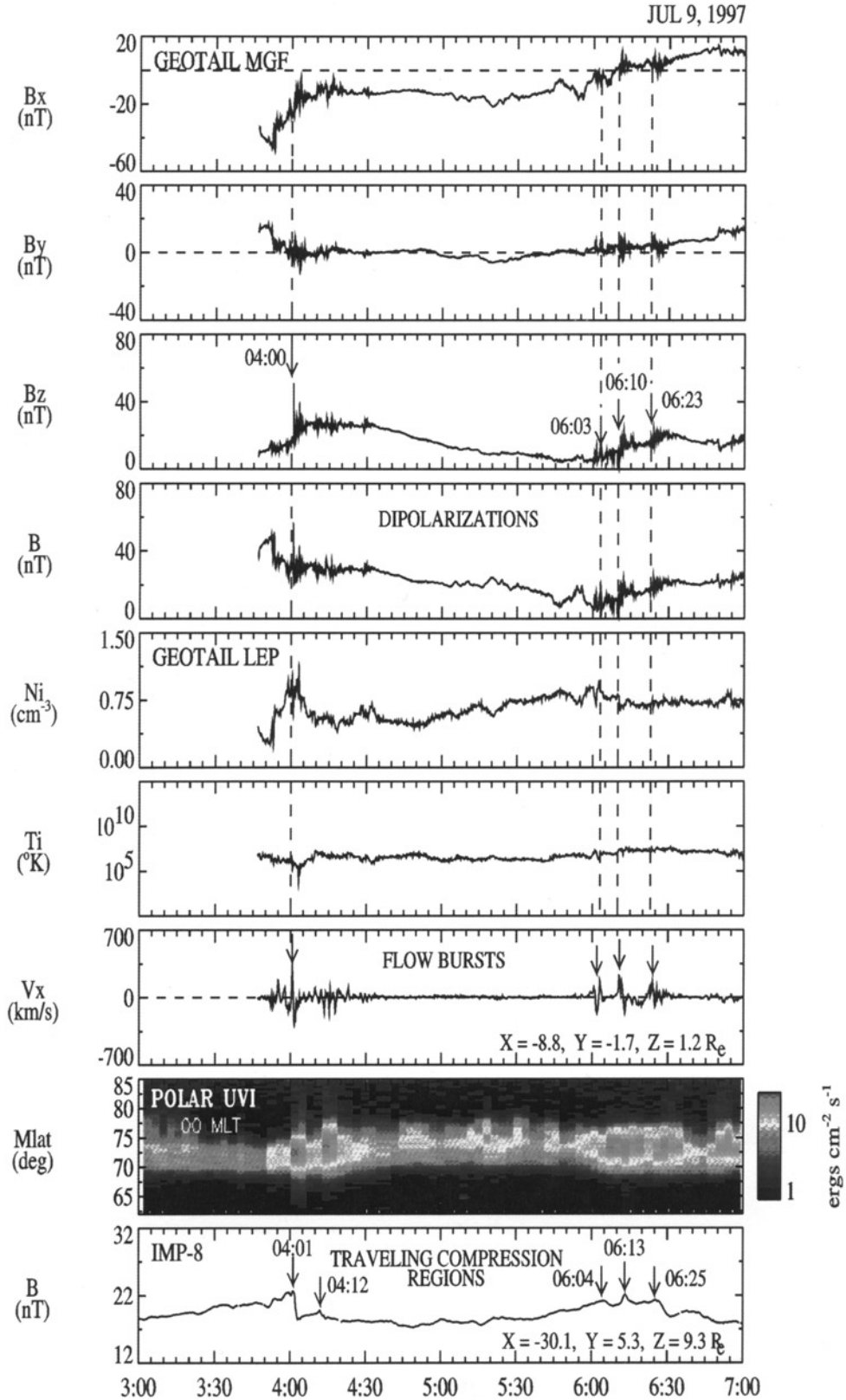

Figure 5. Geotail magnetic field and X component of the plasma flow velocity are displayed in the GSM coordinate system along with ion density and temperature. Vertical dashed lines indicate the times of clear magnetic field dipolarization and plasma flow burst events. Note the close correlation between the dipolarization and flow bursts at Geotail at $X \sim -9\ R_E$ and the TCRs, indicating plasmoid ejection in the IMP 8 magnetic field measurements at $X \sim -30\ R_E$. See color version of this figure at back of this issue.

[23] For these events the Geotail spacecraft was located near the inner edge of the plasma sheet at $\sim -9.2\ R_E$. This close to the Earth, sunward flow bursts are expected already to have been decelerated significantly because of their interaction with the strong magnetic fields in the inner magnetosphere [*Birn et al.*, 1999]. Indeed, the magnitude of these earthward flow bursts can be seen to be only $\sim 250-350$ km s^{-1}. By comparison, at greater downtail distances the magnitudes of such flow bursts are typically twice as great [*Baumjohann et al.*, 1999; *Tu et al.*, 2000], and they are observed, on rare occasions, to reach 2000 km s^{-1} [*Fairfield et al.*, 1998].

[24] The vector variations in the plasma velocity at Geotail, displayed in Figures 6 and 7, also suggest that these observations were taken deep in the braking region. In particular, these impulsive earthward flow bursts, lasting only 1–2 min, are followed by "rebounds" where the plasma speed becomes briefly tailward but with a smaller magnitude. We would argue that as an individual flow burst dissipates, the resulting decrease in the ram pressure exerted upon the inner magnetosphere may allow the inner magnetosphere to rebound slightly as it moves toward a new pressure equilibrium. In addition, the earthward flow bursts are accompanied by a rotation of the flow in the equatorial plane toward the flanks as if the flow were attempting to move laterally around an obstacle, in this case the high field intensity inner magnetosphere. Statistical analysis of the V_y, perturbation accompanying a large number of earthward flow bursts by *Nagai et al.* [2000] have produced a similar pattern of flow diversion.

[25] In Figures 6 and 7 the close relationship between these earthward flow bursts and the dipolarization of the local magnetic field at Geotail is displayed in more detail. As pointed out in previous studies, the earthward flow bursts are accompanied by prompt increases in B_z. However, according to the magnetic flux "pileup" model of the substorm current wedge [e.g., *Shiokawa et al.*, 1998a, 1998b; *Birn et al.*, 1999] the dipolarization does not reach its final inclined state until several minutes later. Indeed, this is the case for both substorms. In Figure 6 a sudden increase in B_z occurs at 0400:40 or about 30 s after the beginning of the earthward flow burst, but B_z does not reach its final plateau for another 3 min. In the case of the second substorm, in particular, it appears that the dipolarization proceeded by "steps," with each flow burst event driving the B_z field to a new, higher level of dipolarization. For the first substorm it is interesting to hypothesize that additional earthward flow bursts in adjacent flow channels may have been responsible for transporting the northward magnetic flux of the inner magnetosphere, which gives rise to its final state of dipolarization. However, such an interpretation is not testable with just the single Geotail spacecraft.

[26] Figures 6 and 7 display the plasma ion beta, the total pressure (i.e., the thermal pressure of the plasma ions plus the magnetic field pressure), and the dynamic or "ram" pressure due to the bulk flow of the ions. The high ratio of $T_i/T_e \sim 5-7$ in the plasma sheet [e.g., *Slavin et al.*, 1985] makes the electron contribution to the thermal plasma pressure small. For the first substorm, Geotail was in the outer plasma sheet, indicated by $\beta_i \sim 1$, and the magnetic field measurements suggest that it was not close to the center of the cross-tail current layer. The thermal pressure of the ions was about 0.5 nPa, which is near the mean thermal pressure of the ions in the plasma sheet near midnight at $X \sim -10\ R_E$ determined from the statistical analysis by *Hori et al.* [2000].

[27] In this case the earthward flow burst has a dynamic pressure of about 0.3 nPa, assuming 10% O^+ and 90% H^+. Unfortunately, the composition of the thermal plasma was not measured. The observed heavy ion composition of the plasma sheet is, in general, quite variable, with the oxygen ion contribution, for example, sometimes exceeding 50%, especially during and just following substorms [*Lennartsson and Shelley*, 1986; *Daglis and Axford*, 1996]. The plasma sheet total pressure responded by first increasing by a similar amount $\sim$0.3 nPa, just ahead of the flow burst, indicative of "snow plowing" and compressional heating. Next, just after the peak dynamic pressure, the plasma thermal pressure experienced a negative excursion relative to the preburst pressure level of ~ -0.3 nPa supporting our suggestion that the plasma sheet earthward of Geotail first compressed because of flow burst and then "rebounded," briefly, as it settled toward its new stress equilibrium.

[28] The Geotail observations during the second substorm are displayed in Figure 7. In this case the spacecraft was much deeper in the plasma sheet as evidenced by the high plasma $\beta_i \sim 10$ and proximity to the cross-tail current layer based upon the reversal of B_x around the time of the middle flow burst. The total pressure was similar to that during the first substorm and dominated by ion thermal pressure consistent with Geotail being near the center of the plasma sheet. As shown in Figure 7, the plasma sheet pressure was driven higher by $\sim 0.1-0.2$ nPa with each succeeding flow burst. Also, a clear compression was observed ahead of each earthward flow burst just as was seen during the first substorm. The ram pressure in each flow burst, with the same assumption of 10% 0^+, was $\sim 0.1-0.15$ nPa, which is less than, but comparable to, the individual increases in the ambient thermal pressure, albeit a small increase in the O^+ fraction of the plasma sheet would bring these pressures into balance. It is also possible that Geotail was near the center of a channel of fast flow in the case of the first substorm but at the edge of a channel for the second substorm, where the flow speed might be reduced. However, a single spacecraft cannot access the expected gradients or shear in these earthward flow channels with local time.

[29] A final aspect of the compressional heating of the central plasma sheet by these flow bursts during this second substorm is their temporal profile. In each case the plasma thermal pressure remains enhanced for $\sim 2-10$ min before it tends to relax back toward its preflow burst level. The B_z component of the magnetic field and the total magnetic field (see Figure 5) increases throughout this interval as the magnetic field dipolarization process continues and the plasma sheet ion beta gradually reduces slightly. Again, this is the behavior predicted by the "flow braking/magnetic flux pile up" scenarios for dipolarization. The field-aligned currents at the dawnward, duskward, and inner boundaries of the SCW are driven by the pressure gradients arising from the compression produced by the flow braking, and they are, in turn, dissipated by giving up energy to these FACs. The observations in Figure 7 would suggest that the characteristic time for the dissipation of the energy carried by individual flow bursts is $\sim$10 min. However, the flow bursts also transport northward magnetic flux to the inner magnetosphere, and it is this process that supports and determines the final degree of dipolarization that is present late in the recovery phase after the SCW has dissipated.

[30] Turning to the magnetic field dipolarization, the GOES and Geotail magnetic field observations during the two 9 July 1997 substorms are compared more closely in Figures 8 and 9, respectively. For the purposes of this comparison the magnetic field measurements from both satellites have been rotated into the *H*, *V*, *D* system, where *H* is antiparallel to the Earth's dipole (i.e., positive northward), *V* is parallel to the magnetic equatorial plane and directed outward from the center of the planet, and *D* completes the right-handed system (i.e., positive toward the east). In addition, the latitude angle of the field in this *H, V, D* system is also calculated and displayed in Figures 8 and 9.

[31] For the first substorm, Figure 8 shows that the dipolarization process at both spacecraft began with an initial "pulse" of enhanced B_H, which was observed first at Geotail at 0400:40 and then $\sim$23 s later at GOES 8. These increases in B_H all reflect changes in the inclination of the magnetic field with the latitude angle at both spacecraft, finally reaching $\sim 45°$ by the end of the interval. Since the two spacecraft were nearly radially aligned and in the premidnight sector, it appears that this initial dipolarization

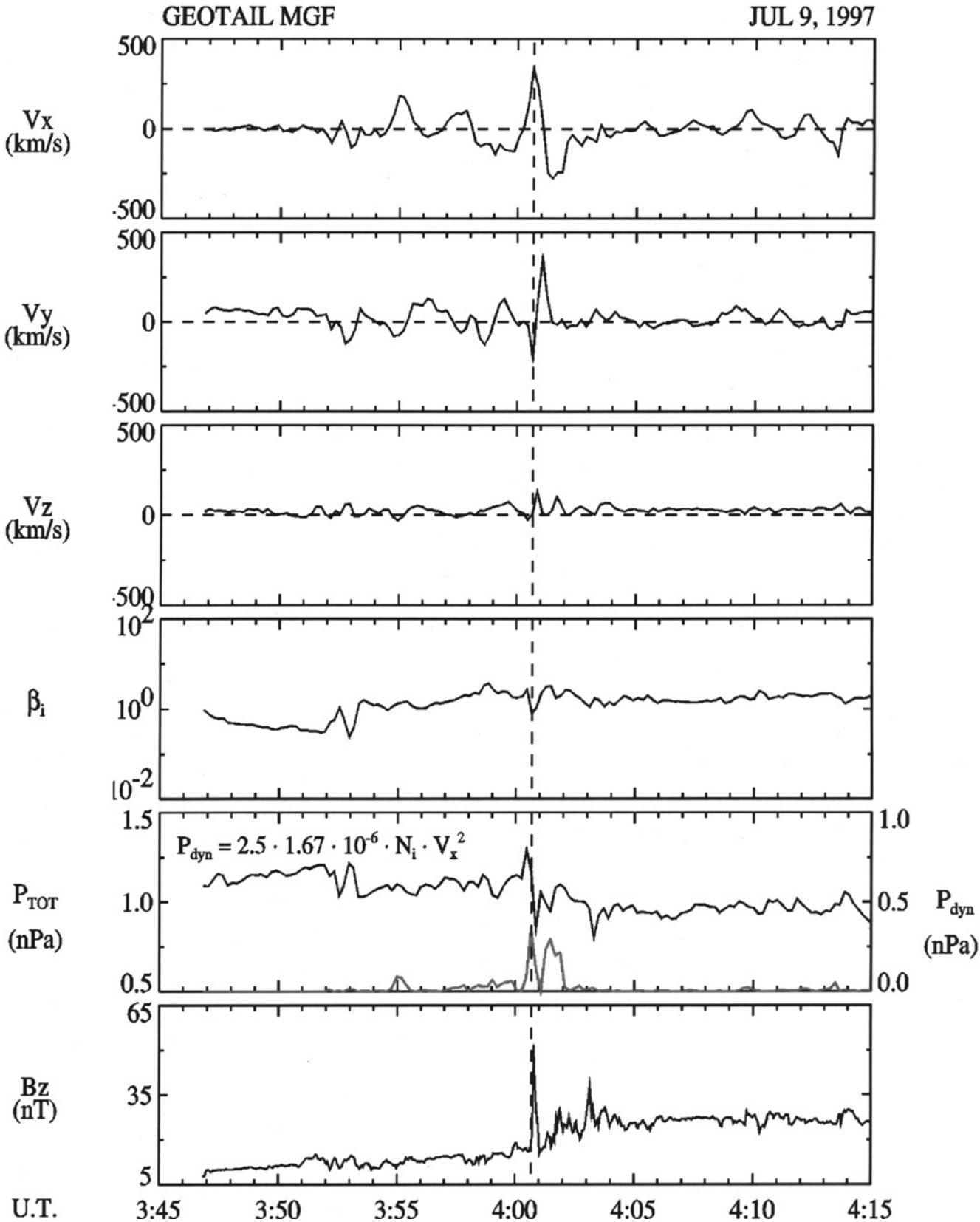

Figure 6. The plasma flow velocity, the plasma ion beta, the total and ram pressures, and the B_z component of the magnetic field are displayed for the first of the substorms under examination. (Note, a plasma sheet composition of 10% O^+ and 90% H^+ has been assumed in calculating the plasma sheet flow ram pressure.) See color version of this figure at back of this issue.

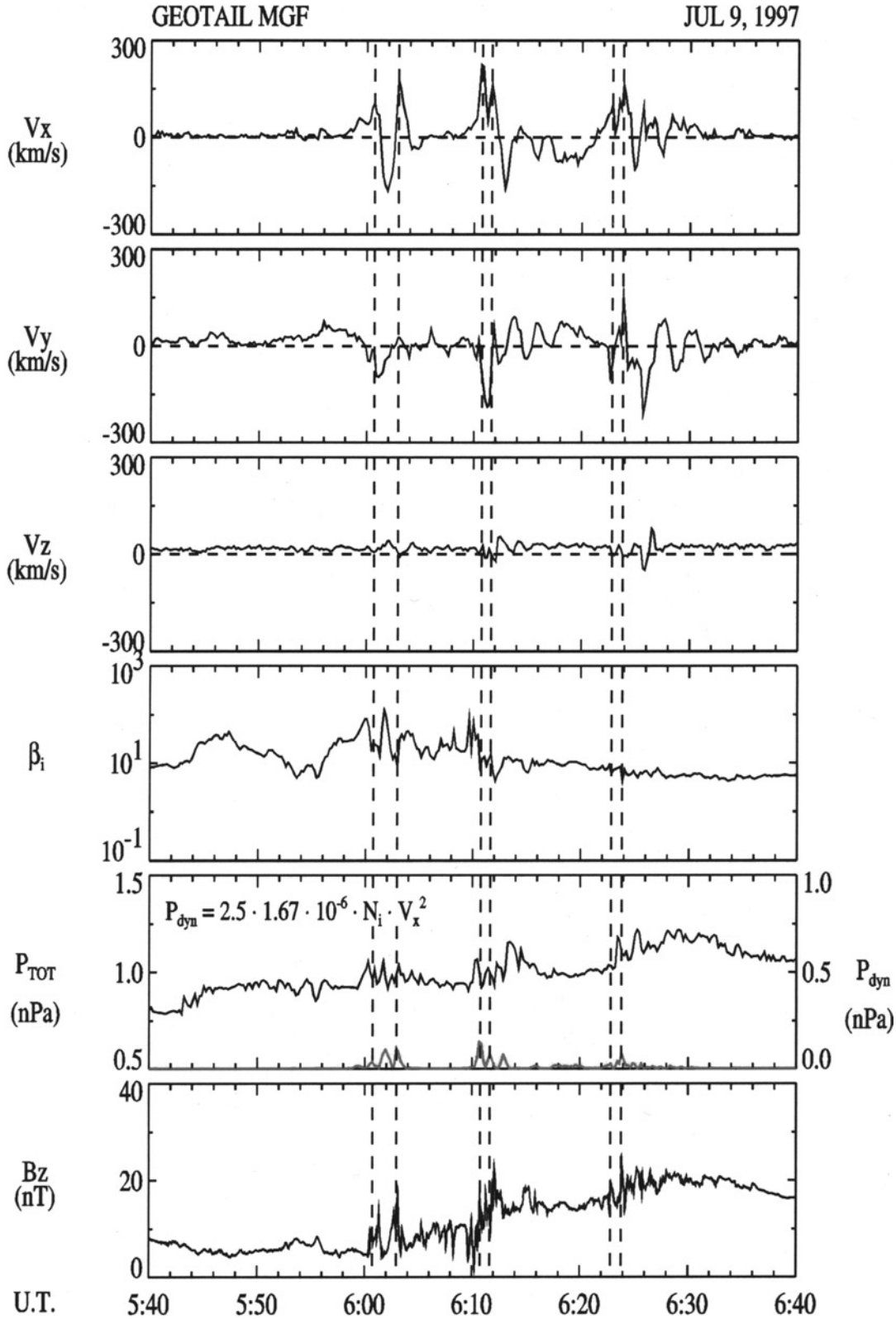

Figure 7. The plasma flow velocity, plasma ion beta, the total and ram pressures, and the B_z magnetic field component are displayed for the second substorm in the same format as in Figure 6. Note the step-like progression of magnetic dipolarization at Geotail. See color version of this figure at back of this issue.

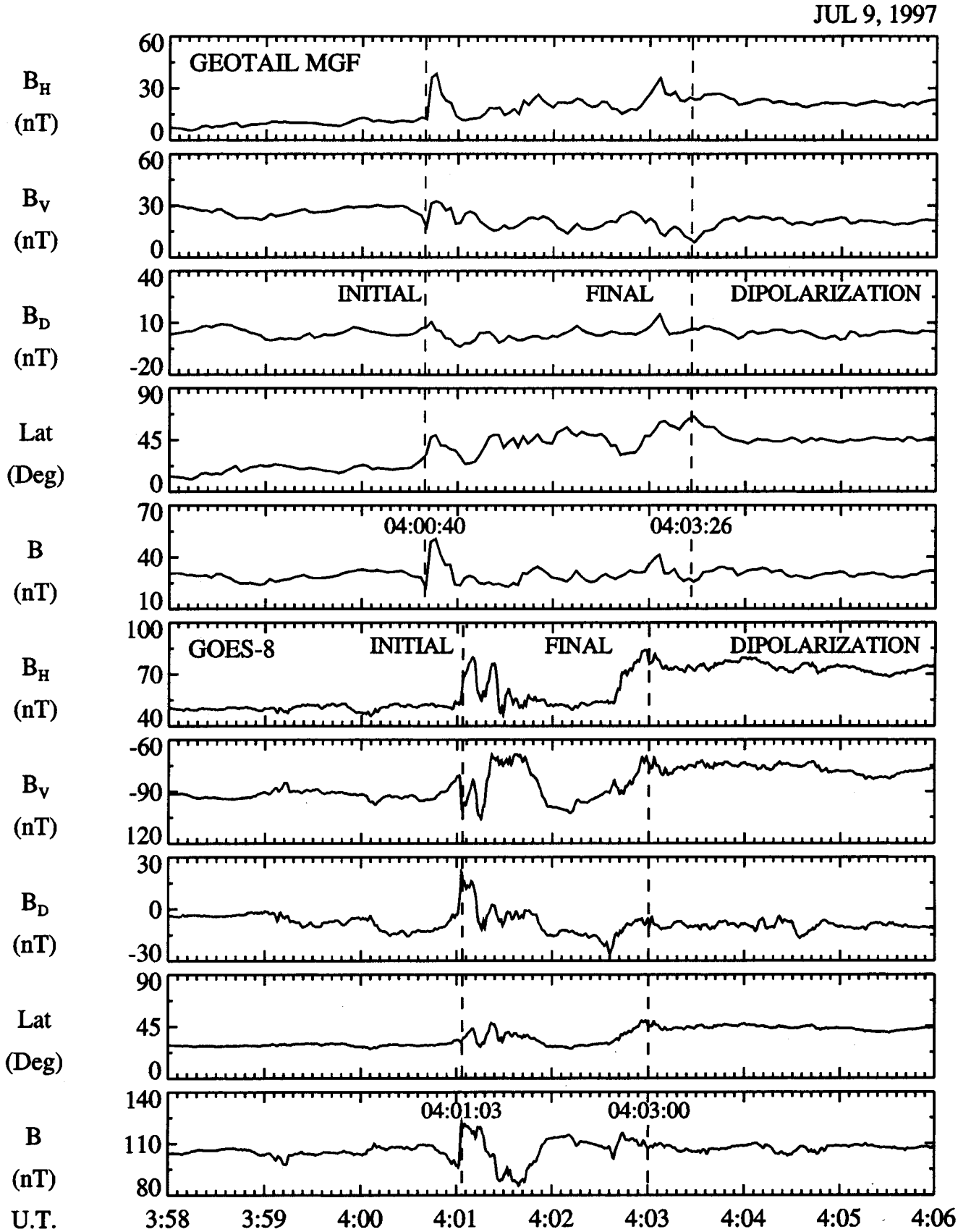

Figure 8. The progression of magnetic field dipolarization at GOES 8 and Geotail for the first substorm is compared using their magnetic field measurements. For convenience both sets of measurements have been rotated into the H, V, D coordinate system.

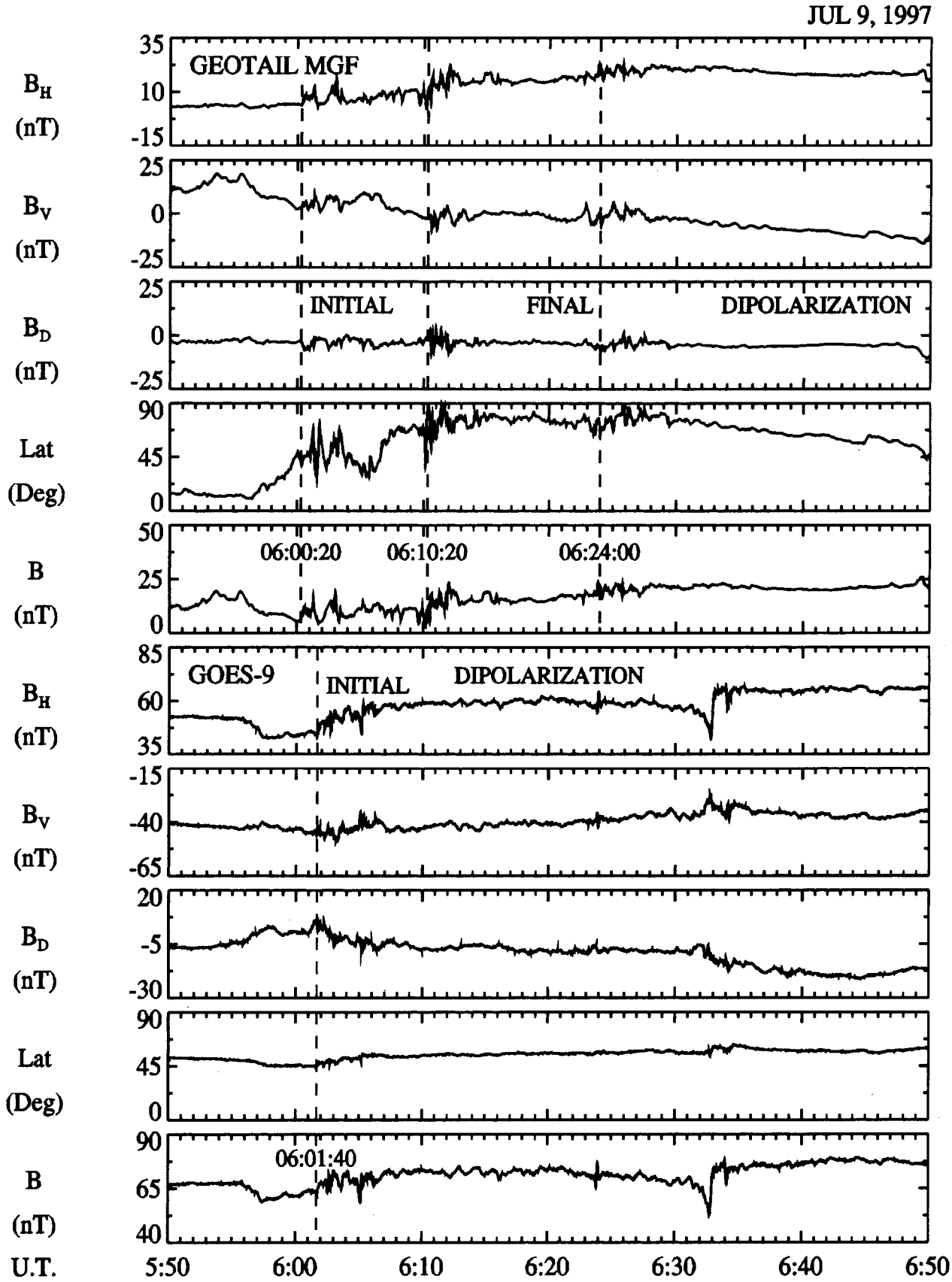

Figure 9. The progression of magnetic field dipolarization for the second substorm at GOES 9 and Geotail is compared using their magnetic field measurements in the same format as in Figure 8.

propagated radially earthward at a speed of $\sim(-6.5 + 9.2\ R_E)/23$ s = 751 km s^{-1}. However, the final dipolarization state was not reached until 0403:00 and 0403:26 at GOES 8 and Geotail, respectively. Hence this final state was observed first at the innermost spacecraft and then propagated, tailward at $\sim(-6.5 + 9.2\ R_E)/26$ s = 665 km s^{-1}. Given the several second uncertainties in assigning the event times, the inward propagation speed of the initial dipolarization and the tailward propagation of the final state are essentially the same at ~700-800 km s^{-1}. These speeds are comparable to the 100–1000 km s^{-1} speeds found in previous studies [e.g., *Jacquey et al.*, 1991].

[32] The dipolarization accompanying the second substorm is examined in Figure 9. The Geotail magnetic field exhibits three pulses or step-like increases in B_H. However, changes in field latitude angle also occur because of plasma sheet motion taking Geotail closer to or farther from the cross-tail current sheet. For example, the increase in field latitude, which begins several minutes prior to the sharp 0600:20 event, is well correlated with a plasma density and β_i increases in Figures 5 and 7. This strongly suggests that this increase in magnetic field inclination was a spatial effect associated with the spacecraft more closely approaching the cross-tail current layer in the central plasma sheet. The latter B_H increases at Geotail, leaving the magnetic field highly dipolarized or nearly antiparallel (90°) to the Earth's dipole, again indicating that the spacecraft was in the cross-tail current layer.

[33] While Geotail and GOES 9 are not nearly as well aligned radially as was the case for the first substorm, it is of interest to see that again, dipolarizattion is first observed at Geotail at $-9.2\ R_E$ and only later at $-6.6\ R_E$ by GOES 9. Because of the nature of the alignment and probable azimuthal propagation delays, it may not be legitimate to compute a Geotail to GOES 9 radial propagation speed, but the result would be $\sim(-6.6 + 9.2\ R_E)/80$ s = 208 km s^{-1}. This effective earthward propagation speed may be aliased toward a lower value because of combining azimuthal and radial propagation delays, but the result is still of the order of the speed inferred for the first substorm. More significant, however, is the fact that the magnetic field at GOES 9 reaches its final dipolarized state ~20 min before the magnetic field reached its maximum latitude at Geotail. As with the first substorm, both the earthward propagation of the initial dipolarization and the tailward propagation of the final state are consistent with MHD simulations of the flow braking/magnetic flux pileup model of substorm current wedge formation [*Hesse and Birn*, 1991; *Birn et al.*, 1999].

7. Deep Tail: Traveling Compression Regions

[34] The IMP 8 magnetic field observations on 9 July 1997 are shown in fuller detail in Figure 10. The strong, low-variance magnetic fields oriented predominantly in the $+X$ direction clearly demonstrate that this spacecraft was in the north lobe of the tail for the entire 4 hour interval. As discussed earlier, growth phase loading and expansion phase unloading is plainly evident with the expected close correlation with the polar cap area and the substorm phase. During these loading phases the flaring of the tail is evident in the steady decreases in B_z. These loading intervals end with the initial plasmoid ejections, indicated by TCRs, which take place at 0401:30 and 0411:50 and 0604:40, 0613:00 and 0624:40 for the first and second substorms, respectively.

[35] TCRs are identified in the far tail by a several minute increase in the lobe field intensity, a mean amplitude of ~10%, and a correlated bipolar $\pm\Delta B_z$ field variation [*Slavin et al.*, 1993]. However, as discussed earlier, if a spacecraft is closer to the NENL and either directly below or above the plasmoid whose central "bulge" is still forming, then only a "partial" TCR will be observed with a weak or absent $+\Delta B_z$ perturbation followed by the usual $-\Delta B_z$ signature [see *Slavin et al.*, 1999]. These partial TCRs are very common at IMP 8 [*Taguchi et al.*, 1997] because this spacecraft crosses the tail at $X \sim -28$ to $-38\ R_E$, where plasmoids are still growing rapidly and accelerating tailward [*Ieda et al.*, 1998; *Slavin et al.*, 1999]. The 9 July TCRs are very similar to those studied previously in the IMP 8 data, with only the first TCR, at 0401:30, displaying the complete $\pm\Delta B_z$ perturbation. The duration of this TCR was ~80 s. The speed of the underlying plasmoid was not measured directly. However, if the mean downtail plasmoid speed of ~300 km s^{-1} determined by Geotail [*Ieda et al.*, 1998] is assumed, then the implied length of the underlying plasmoid was ~4 R_E. This is in good agreement with direct measurements of plasmoid length in the near tail [*Ieda et al.*, 1998].

[36] Finally, it is common for individual substorms to eject more than one plasmoid during their expansion phases [*Richardson et al.*, 1987; *Slavin et al.*, 1992, 1993]. These two substorms are typical, with the first producing two and the second ejecting three plasmoids. The spacing between the TCRs, around 10 min, is comparable to the mean separations between TCRs observed in previous surveys [*Slavin et al.*, 1993].

8. Analysis of NENL Time of Formation and Location

[37] The tail segment of the modern NENL model of substorms is depicted in Figure 11. Reconnection between the open field lines in the north and south lobes of the tail produces high-speed flows in the central plasma sheet, which transport newly closed magnetic flux tubes earthward and compress the dipolar inner magnetosphere. This leg of the substorm process is convective in nature, and the time delay between the onset of open field line reconnection at the NENL and the initial compression of the inner magnetosphere should be

$$\Delta T \sim D/V_E \sim 10R_E/500\,\mathrm{km\ s^{-1}} \sim 2\,\mathrm{min}, \qquad (1)$$

where D is the distance from the NENL to the inner edge of the plasma sheet and V_E is the average flow speed of the earthward flow burst in the central plasma sheet. On the basis of the distributions of NENL locations from *Nagai et al.* [1998] the value of D could be as great as 20 R_E or as small as 5 R_E. The convective speed V_E will decrease as the flow snowplows into the very slowly convecting plasma closer to the Earth [e.g., *Baumjohann et al.*, 1999]. If the flow burst starts out at ~1000 km s^{-1} and brakes to a value $\ll$100 km s^{-1} after covering a distance of 10 R_E, then the mean speed would be ~500 km s^{-1}.

[38] Again, returning to Figure 11, the braking of the earthward flow burst is thought to generate the well-known Pi2 ULF waves, the field-aligned currents that form the upward/downward legs of the substorm current wedge and serve as the ultimate source of the downward precipitating electrons that produce the auroral substorm emissions [*Shiokawa et al.*, 1998a, 1998b; *Birn et al.*, 1999; *Kepko and Kivelson*, 1999]. The additional time delay for the propagation of Pi2s from the inner edge of the plasma sheet to the surface of the Earth is

$$\Delta T \sim d/C_A < 10R_E/1000\,\mathrm{km\ s^{-1}} \sim 1\,\mathrm{min}, \qquad (2)$$

where C_A is the Alfven speed along flux tubes linking the inner edge of the plasma sheet to the Earth. Again, a range of values could be selected for this calculation [e.g., *Moore et al.*, 1987; *Fujita et al.*, 2000]. However, by selecting a rather modest Alfven speed and a maximum propagation distance to the ionosphere the result is an upper limit on the time delay for forming or altering the intensity of the substorm current wedge. The resultant maximum delay, ~1 min, is much less than the typical convective delay for flow bursts to reach the inner magnetosphere from the NENL calculated earlier.

[39] Given these simultaneous observations of the effects of reconnection both earthward and tailward of the NENL on 9 July

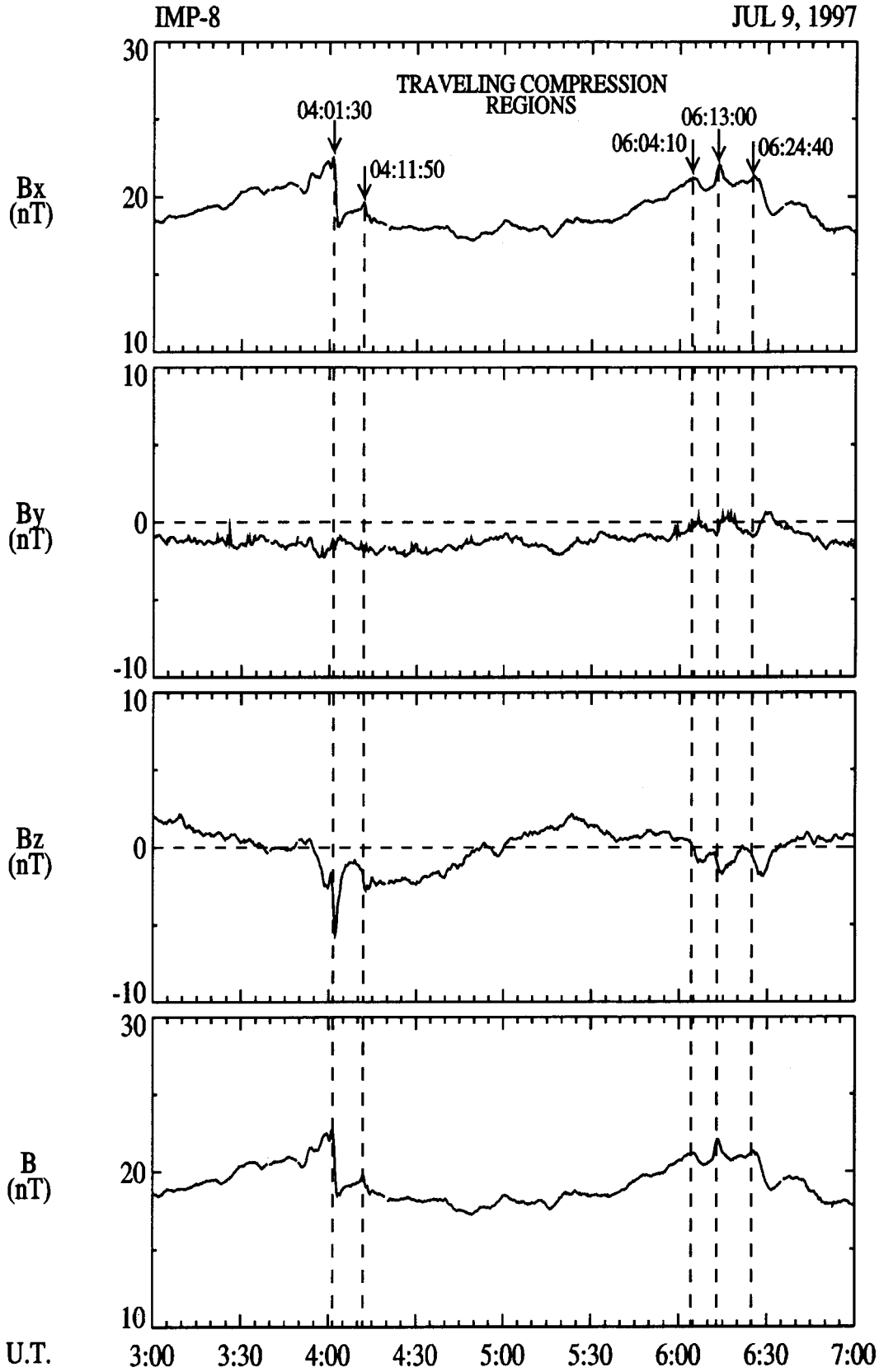

Figure 10. The magnetic field measured by IMP 8 in the north lobe of the magnetotail on 9 July 1997 is displayed in GSM coordinates. Note the occurrence of multiple TCRs near the peak in the loading–unloading process for each substorm.

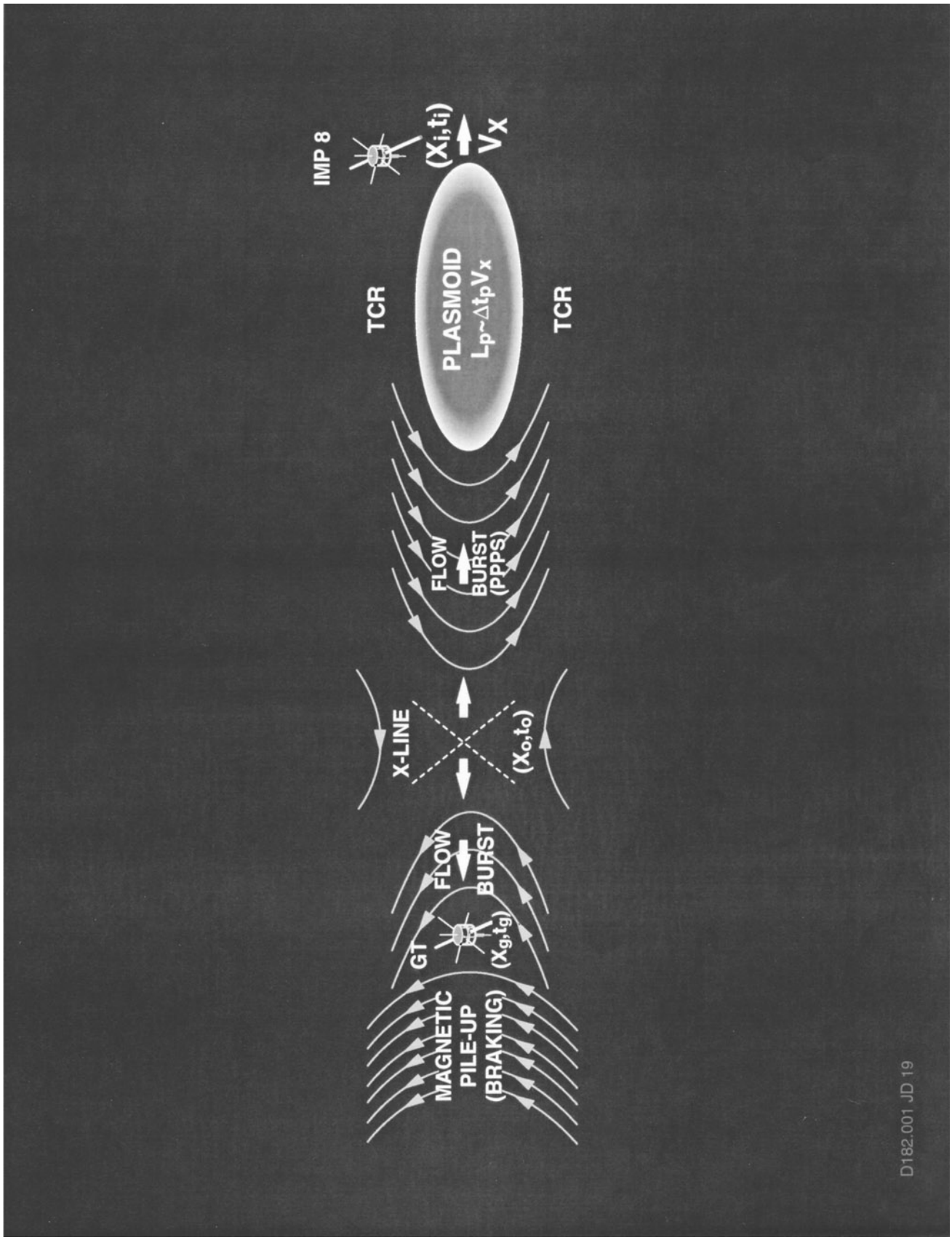
IMP 8
(X_i,t_i)
V_X
TCR
PLASMOID
$L_p \sim \Delta t_p V_x$
TCR
FLOW
BURST
(PPPS)
X-LINE
(X_o,t_o)
FLOW
BURST
GT
(X_g,t_g)
MAGNETIC
PILE-UP
(BRAKING)
D182.001 JD 19

Table 1. NENL Onset and Location

V_x, km s^{-1}	t_g, UT	t_i, UT	X_g, R_E	X_i, R_E	X_o, R_E	t_o, UT
500	0359:50	0401:30	−9.2	−30.7	−18.4	0357:51
300	0602:40	0604:10	−8.8	−30.1	−16.3	0559:59
300	0610:20	0613:00	−8.7	−30.1	−14.7	0608:13
300	0623:00	0624:40	−8.6	−30.1	−16.0	0620:22

1997, we can go one step further and, with suitable assumptions, construct a simple one-dimensional model of plasma sheet flow to infer the time t_o and location X_o at which the reconnection of open lobe magnetic flux begins. We will assume, for simplicity, that the NENL is stationary for some minutes after the onset of open field line reconnection. Furthermore, the tailward flow speed will be set equal to the ~300 km s^{-1} mean plasmoid speed observed by *Ieda et al.* [1998] in this region of the tail. If the earthward and tailward flow speeds have magnitudes V_E and V_t, then t_o and X_o may be directly calculated from the location and arrival time of the earthward flow burst at the Geotail spacecraft, X_g and t_g, and the time location of the peak of the TCR at IMP 8 X_i and t_i, as follows:

$$t_o = \left[V_E t_g + V_t t_i\right]/[V_E + V_t] + \left[X_i + L - X_g\right]/[V_E + V_t] \quad (3)$$

$$X_o = V_t[t_i - t_o] + [X_i + L]. \quad (4)$$

The parameter L is the half length of the plasmoid along the Sun-Earth axis, which we set equal to 2 R_E on the basis of the statistical analysis of the Geotail observations by *Ieda et al.* [1998]. Utilizing the braking rates determined in previous analyses [*Baumjohann et al.*, 1999; *Tu et al.*, 2000], the average earthward speed V_E should be ~20–30% greater than the flow burst speed measured in situ by Geotail at ~9 R_E. Accordingly, we have taken $V_E \sim$ 500 km s^{-1} for the first substorm and ~300 km s^{-1} for the second, where the flow burst speeds were somewhat slower.

[40] In this manner we have calculated X_o and t_o for the earthward flow burst-plasmoid pairs observed at ~0400–0401, 0603–0604, 0610–0613, and 0623–0625. The results are shown in Table 1. No neutral line location and onset time can be calculated for the second plasmoid of the first substorm as no clear earthward flow burst was recorded at Geotail. The location of the NENL along the X axis for the first substorm was $X \sim -18.4$ R_E as opposed to $X \sim -16.3$, -14.7, and -16.0 R_E for the reconnection events in the second substorm. The onset time for open flux tube reconnection preceded the arrival of the flow bursts at Geotail by ~2–3 min. Overall, these time delays are very close to the estimates we derived from the NENL model using (1). Finally, error analysis of (3) and (4) and the input parameters indicates that the uncertainties in the time of lobe flux reconnection and location are ~±1 min and ±1–2 R_E, respectively.

[41] The downtail distances of ~−15 to −18 R_E inferred for these substorms are somewhat closer than the typical −20 to −30 R_E range determined by *Nagai et al.* [1998], *Machida et al.* [1999], *Baumjohann et al.* [1999], and *Miyashita et al.* [2000] on the basis of statistical analyses of Geotail plasma sheet flow velocities and ground observations of substorm expansion phase onsets. However, at least one example of reconnection in the tail near $X \sim -14$ R_E in the tail was analyzed in detail by *McPherron and Manka* [1985]. Indeed, as discussed earlier, this result was expected because our events required that IMP 8 detect the tailward passage of a plasmoid and previous studies strongly suggest that this is possible only when the NENL forms closer than normal to the Earth [*Taguchi et al.*, 1997].

9. Substorm Timescales

[42] The challenge in observationally determining the temporal and spatial evolution of substorms in the magnetotail lies only partially in obtaining fortuitous alignments of spacecraft and instruments. It is also necessary to assign accurate propagation speeds to each of the substorm phenomena that will allow them all to be registered in a common time and space framework. The reason this latter issue is so important is that in general, the physical phenomena, for example, bulk plasma flows, energetic particle enhancements, Pi2 waves, etc., are rarely measured at their point of origin. In nearly all cases they have to propagate some distance before they encounter the instrument that takes their measure. These delays add noise and dispersion into studies of when a given process or phenomena occurs relative to substorm expansion onset. For example, the time of arrival of a fast earthward flow at a near-tail spacecraft such as Geotail is often taken as an estimate for the time when lobe field line reconnection commenced. Yet, depending upon the relative distance of the spacecraft from the NENL (see Figure 11), the actual time of onset for lobe field line reconnection could have been up to ~5–10 min earlier depending upon the range of possible distances and flow speeds.

[43] Similarly, *Slavin et al.* [1992, 1993], during the course of analyzing large numbers of plasmoid and TCR events, found that onset determined by AKR intensification preceded, on average, the Pi2 and *AL* index onsets by only ~1–2 min, while those determined from energetic electron injections at geosynchronous orbit were preceded ~3–5 min. The reason for the larger delays using the charged particle observations is, of course, the relative slowness of particle drifts compared with MHD wave and FAC propagation speeds. More recently, a detailed study of the temporal relationship between expansion onset in Polar UVI auroral images and Pi2 waves was conducted by *Liou et al.* [2000a]. Likewise, they found that Pi2 onsets are delayed by 1–3 min relative to the auroral imaging and attributed the delays to the MHD propagation times from their origins in the near-tail to ground stations at various points around the globe, much as we have done with (2). In a second study, *Liou et al.* [2000b] found that AKR enhancements were, indeed, coincident with UVI onsets to within the ~±1 min uncertainty of the auroral measurements.

[44] The ISTP observations of the two 9 July 1997 substorms analyzed in this study are summarized in Figures 12 and 13 and Table 2. Auroral breakup first appears in the UVI keogram at 0400, but as discussed earlier, the temporal resolution of the data in this display is only 3 min. However, the 0400 onset time is supported by the 1 min resolution measurements from the Polar Ionospheric X-ray Imaging Experiment (PIXIE) [*Imhof et al.*, 1995]. In Figure 12 the 8–12 keV X-ray counts emanating from the auroral bulge region have been integrated over 1 min. As shown, there is a strong intensification in the X-ray flux at 0400. Figure 12 also shows the 0359:50 earthward flow burst at Geotail and 0401:30 plasmoid passage by IMP 8, which allowed us to infer the formation of the NENL at 0357:61 (i.e., the vertical dashed line). Hence the times necessary for the flow out of the NENL to reach the inner magnetosphere at $X \sim -9$ R_E and the deep tail at $X \sim -31$ R_E were ~2 and 3.5 min, respectively. The brightening and poleward expansion of the premidnight aurora, the enhancement of the AKR emissions, the observation of the Pi2 pulsations at Hermanus, South Africa, and the high-latitude negative magnetic bay at Fort Churchill, Canada, were all observed within ~1 min of the arrival of the flow burst at Geotail. This implies, as discussed earlier, that the

Figure 11. (opposite) Meridian cut through the central tail showing the earthward and tailward consequences of the onset of open field line reconnection; earthward and tailward high-speed flows, flow braking and dipolarization, and plasmoid ejection. See color version of this figure at back of this issue.

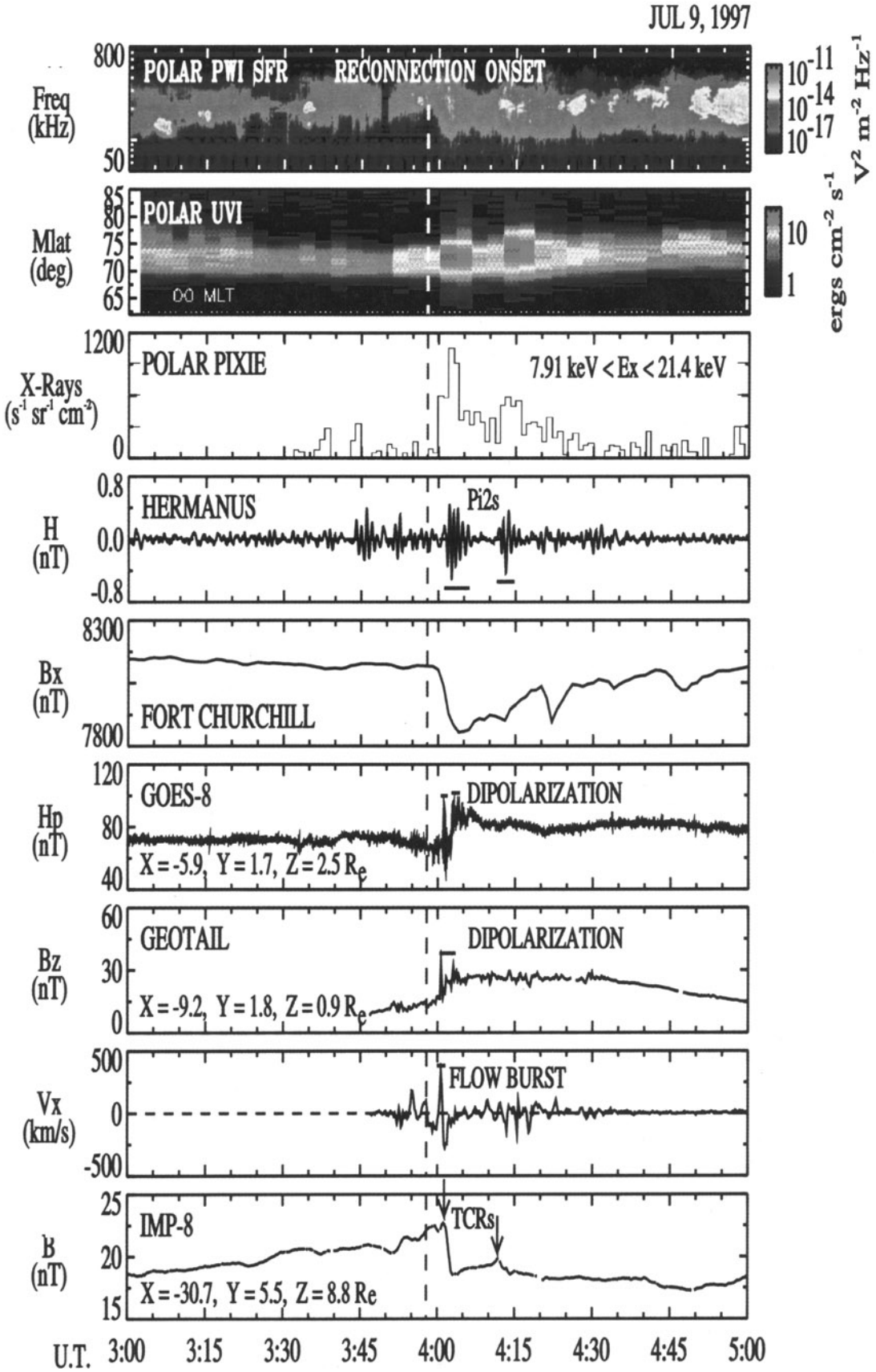

Figure 12. A summary of the ISTP observations for the first substorm is presented with a vertical dashed line marking the inferred time of the onset of lobe field line reconnection at the NENL. See color version of this figure at back of this issue.

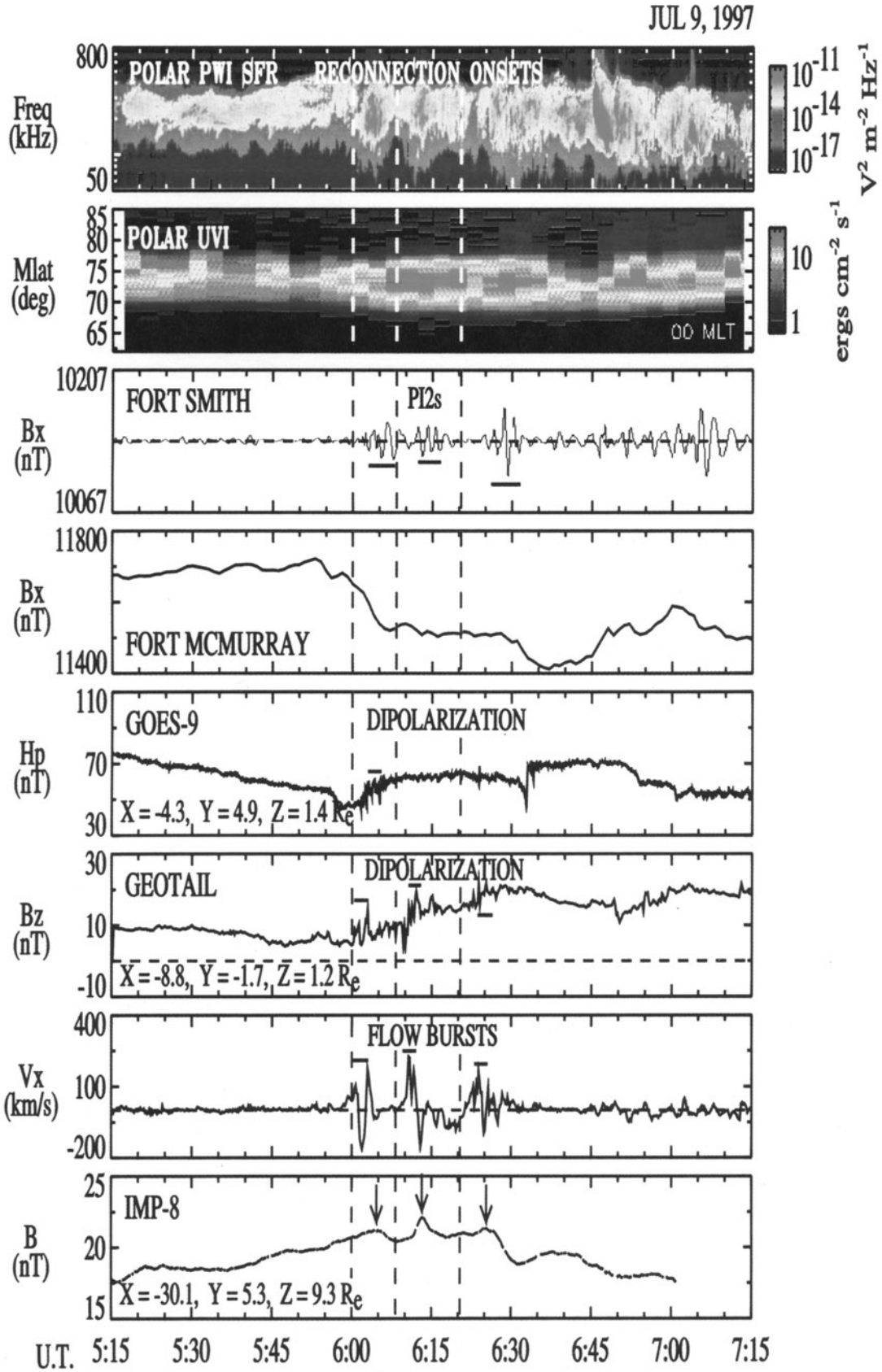

Figure 13. A summary of the ISTP observations for the second substorm is presented with vertical dashed lines marking the inferred times for the onset of lobe field line reconnection at the NENL associated with each episode of earthward flow bursts. See color version of this figure at back of this issue.

Table 2. Substorm Spatial and Temporal Evolution

	Substorm 1		Substorm 2					
	Time, UT	X, R_E	Time, UT	X, R_E	Time, UT	X, R_E	Time, UT	X, R_E
NENL	0357:51 ± 1 min	−18.4 ± 2	0559:59	−16.3	0608:13	−14.7	0620:22	−16.0
Flow burst	0359:50 ± 20 s	−9.2	0602:40	−8.8	0610:20	−8.7	0623:00	−8.6
Substorm	0400 ± 1 min	···	0602	···	0611	···	0625	···
Plasmoid	0401:30 ± 10 s	−30.7	0604:40	−30.1	0613:00	−30.1	0624:40	−30.7

transfer of energy from the braking of the flow burst to the ionosphere occurs on timescales consistent with the Alfven propagation speed in the high-latitude magnetosphere. Finally, we note that although there was not a clear flow burst signature at Geotail at the time of the second IMP 8 TCR, there was a second auroral intensification and poleward expansion, a second AKR enhancement, and a suggestion of a second Pi2. Hence it could be speculated that a second flow burst occurred for which Geotail was located too far dawnward or duskward to detect, but this hypothesis is not testable with just the single spacecraft.

[45] Figure 13 summarizes the strong correlation between the three flow bursts and three plasmoids ejected down the tail, as inferred from the three TCRs they produced, during the second substorm. These three flow bursts also generated three well-defined Pi2s, and although less clear, the auroral emissions and AKR also show some indication of three enhancements. The onset times for lobe flux tube reconnection inferred from the correlated flow bursts and plasmoid ejections are indicated with vertical dashed lines at 0559:59, 0608:13, and 0620:22. The spatial and temporal evolution of the second substorm is very similar to the earlier one. The propagation times from the NENL to the earthward flow bursts at Geotail were 3, 2, and 3 min, respectively. The longer delay times relative to the first substorm are consistent with lower velocity of the flows measured at Geotail during the earthward flow bursts. The brightening and poleward expansion of the premidnight aurora, the enhancement of AKR emissions, the observation of the Pi2 pulsations at Fort Smith and the high-latitude negative magnetic bay at Fort McMurray, and the arrival of the flow burst at Geotail were all observed between 0602 and 0603. For the two subsequent episodes of lobe flux tube reconnection, commencing at ∼0608 and 0620, near-simultaneous Pi2 and AKR enhancements are observed at 0611 and 0625, respectively. The intensity of the field-aligned currents linking the low-latitude magnetosphere and the auroral zone appears to have continued to increase until 0645–0700 on the basis of the intensity of the AKR and the depth of the high-latitude negative bay at Fort McMurray. The continued development of the expansion phase is also consistent with the tail unloading profile in the IMP 8 data. The tail lobes did not complete their unloading until around 0700. Following the arguments of *Baumjohann et al.* [1999], it is likely that the substorm drew to a close because the third the final NENL was forced to retreat tailward by the tailward expansion of the region of dipolarized magnetic fields in the plasma sheet.

[46] The temporal association between all of the different substorm phenomena displayed in Figures 12 and 13 argues strongly for the two substorm propagation timescales discussed earlier: one based upon the braking of the earthward flow bursts and the other upon the propagation of changes in the SCW current system. In general, the plasma sheet flow speeds measured during the flow bursts range from ∼1 to 10 R_E per minute. If the NENL forms at, say $X \sim -20$ R_E, then its effects will be observed at $X \sim -10$ and -30 R_E after 1–10 min, respectively. This is in good agreement with the 2–3 min delays we derived for 9 July 1997 substorms analyzed here. This is the first timescale for the substorm process associated with convection speed of the flow bursts emanating from the NENL.

[47] The second timescale is associated with the propagation of the field-aligned currents, which define the substorm current wedge [*McPherron et al.*, 1973]. It is this system of FACs that transfers energy from the earthward flow bursts in the braking region, earthward of $X \sim -12$ or -13 R_E. It is these field-aligned currents that give rise, ultimately, to the low-altitude double layers that accelerate electrons down into the auroral oval to produce the auroral bulge. The Alfvenic propagation time for the creation or modification of FACs linking the equatorial regions of the inner magnetosphere and the high-latitude ionosphere is known from both in situ measurements and Pi2 pulsations to be ∼1000 km s^{-1} [*Fujita et al.*, 2000; *Moore et al.*, 1987]. The values we derived from the time it took for the effects of dipolarization to move from Geotail at $X = -9.2$ R_E to geosynchronous orbit, ∼700 km s^{-1}, are in reasonable agreement with this speed. Hence this second timescale associated with the propagation of energy from the equatorial region of the inner magnetosphere where flow burst-fed pressure gradients drive field-aligned currents down to the high-latitude ionosphere to form the substorm current wedge is only ∼10 R_E/1000 km s^{-1} = ∼ 1 min. Accordingly, the two timescales, the first convective and the second Alfvenic, were separated by only a factor of ∼2 or 3 in the delays they introduce into the timing of substorm features for the events analyzed here.

10. Conclusions

[48] The most important new results presented here are the detection of the simultaneous earthward flow bursts and the tailward plasmoid ejection predicted by the NENL model and the use of this information to infer the time and location at which open field line reconnection commenced. While both phenomena have been well studied and related to expansion phase onset separately, this study is the first to confirm the expected close correlation between earthward flow bursts and tailward plasmoid ejection for individual substorms. To our knowledge, only one other example of near-simultaneously flow burst-plasmoid ejection has been reported previously [*Petrukovich et al.*, 1998]. We have presented four more examples and gone on to demonstrate how they can be used to infer NENL location and the time of lobe field line reconnection. Overall, our two substorms show that each episode of near-earth neutral line formation, and there may be several during the course of a single substorm, results in the fast flow of plasma, both earthward and tailward, in the form of spatially and temporally compact flow bursts and plasmoids.

[49] The results of our simple one-dimensional model are based upon the use of a mean earthward flow scaled from the plasma measurements in the earthward flow burst and a fixed plasmoid ejection speed of 300 km s^{-1} based upon the results of *Ieda et al.* [1998]. They indicate, as shown in Tables 1 and 2, that lobe field line reconnection began several minutes before the earthward flow bursts reached at Geotail at $X \sim -9.2$ R_E and plasmoids passed IMP 8 at $X \sim -30$ R_E. The locations of the NENL for both substorms were near $X \sim -15$ to -18 R_E with an uncertainty of ±1–2 R_E. This value is just slightly less than the typical ∼−20 to −30 R_E distances derived from plasma sheet flow data by *Nagai et al.* [1998] and plasmoid formation by *Ieda et al.* [1998]. However, for this study such a bias toward substorms with closer than typical NENL locations was anticipated because our event selection criteria admitted only events for which TCRs were detected at IMP 8.

[50] In addition, our results also bear on issues relating to tail dynamics during substorms that exhibit multiple onsets or intensifications such as the second of the two substorms studied here. For the 0602 substorm, there appear to have been three separate episodes of reconnection. All three resulted in the production of earthward flow bursts and tailward ejection of plasmoids. Similar neutral line locations of $X \sim -15$ to -16 R_E were inferred with delay times of ~2–5 min between the commencement of lobe flux tube reconnection and the observation of dipolarization, Pi2s, enhanced AKR emissions, and high-latitude negative bays. The temporal separation of ~9–14 min between each intensification is well within the typical range of separations between multiple plasmoids in the deep tail [*Slavin et al.*, 1993]. Taken together, these results suggest that multiple episodes of NENL formation and retreat may be common during more intense, longer-duration substorms. In turn, this may be the ultimate reason why approximately two thirds of plasmoids in the deep tail are observed in groups of two or more separated by ~10–20 minutes [*Slavin et al.*, 1993].

[51] As schematically portrayed in Figure 11, bulk flow energy is converted in the inner magnetosphere to plasma sheet heating, energetic particle acceleration (not studied here), and the field-aligned currents, which create the substorm current wedge. It is these field-aligned currents generated in the braking region that lead to the formation of auroral double layers and the downward acceleration of electrons at low altitudes to produce the well-known substorm auroral bulge and expansion. The propagation time for the development of these field-aligned currents should be similar to the Alfven speed, i.e., $\sim 10^3$ km s^{-1}. This is supported by our observations that earthward of Geotail, the substorm onset indicators are simultaneous to within ±1 min, indicating that the substorm current wedge develops and transfers energy and momentum on the much faster timescale of Alfven waves traveling between the low-latitude magnetosphere and the auroral zone. The existence of these two timescales for the development of the substorm expansion phase is also among the key predictions of the modern NENL model of magnetospheric substorms [e.g., *Shiokawa et al.*, 1997].

[52] The 9 July 1997 substorms have also provided an opportunity to study the braking of earthward flow burst in the inner magnetosphere and the dipolarization of the magnetic field to produce the substorm current wedge. Our observations indicate that the observation of an earthward flow burst in the inner magnetosphere is always accompanied by an enhancement in the B_z component of the local magnetic field. Comparison between Geotail and GOES 8 and 9 at similar local times shows that this initial dipolarization of the magnetic field propagates from the outer spacecraft to the inner spacecraft with a speed of ~700 km s^{-1}. This speed is near the equatorial Alfven speeds typical of the inner magnetosphere [*Fujita et al.*, 2000; *Moore et al.*, 1987]. However, it is the magnetic field at the innermost spacecraft, i.e., GOES, which achieves its final dipolarization state first, and this state propagates down the tail. These results are highly supportive of the so-called "magnetic pileup" model of the formation of the substorm current wedge [*Hesse and Birn*, 1991; *Shiokawa et al.*, 1997, 1998a, 1998b; *Birn et al.*, 1999]. The transport of magnetic flux proceeds from the tail inward, but this effect eventually leads to the development a region of near-stagnated hot plasma on dipolarized flux tubes in the inner magnetosphere that expands in local time and tailward as later flow bursts continue to provide a source of newly closed flux tubes [e.g., *Baumjohann et al.*, 1999].

[53] We have also used this fortuitous radial alignment of spacecraft to investigate how the interaction of these earthward flow bursts affects the stress balance between the plasma and magnetic fields in the braking region. A rigorous evaluation of stress balance is not generally possible with a single spacecraft because the magnetic curvature force cannot be determined without multipoint measurements. Furthermore, as the thickness of the plasma sheet responds to the changes in magnetic field topology and flow bursts caused by reconnection, a given spacecraft will find itself at progressively different distances relative to the center of the cross-tail current layer because of these changes. The earthward flow burst during the first substorm reached Geotail when the spacecraft was located in the outer plasma sheet (i.e., B_x was relatively strong, and β_i was ~1). In this case the ~0.3 nPa ram pressure associated with the flow burst produced a corresponding ±0.3 nPa compression and rebound of the ambient total plasma and magnetic field pressure. Later, the total pressure decreased until it was comparable to the lobe pressure. The second substorm was similar, but Geotail was located deep in the central plasma sheet near the cross-tail current layer with $\beta_i \sim 10$. Again, dipolarization and an enhancement of the total pressure accompany each flow burst. The ram pressure of the flow bursts, for an assumed O^+ fraction of 10% (not measured), was 0.1–0.2 nPa or just slightly smaller than the observed total pressure increases. Each increase in total pressure tended to dissipate partially on a timescale of ~10 min following each flow burst, but the overall effect of these flow bursts was to increase the total pressure in the central plasma sheet by a factor of about one third by the end of the interval. It is this enhancement of total pressure in the central plasma sheet that ultimately drives the development of the substorm current wedge in the NENL model.

[54] In closing, many important questions concerning the nature of the reconnection process in the tail and its role in magnetospheric storms and substorms remain unanswered. Examples include what is the kinetic dissipation mechanism for "breaking" the field lines in the diffusion region, why reconnection produces such temporally and spatially limited bursty flows, why the NENL forms where and when it does, what determines how many times neutral lines form during a single substorm, what is the global two-dimensional flow field for the plasma sheet, and what factors control the formation and ejection of multiple plasmoids. While future analysis of the ISTP observations will doubtless produce important new results, major leaps forward will probably be limited by the sparseness of the available measurements. On the earthward side it is anticipated that the remote sensing missions such as Imager for Magnetopause to Aurora Global Exploration Mission (IMAGE) may provide powerful new insights into the dynamics of the flow-braking region. However, many aspects of reconnection in the tail and its effects over the global plasma sheet will have to await results from multispacecraft missions, such as the European Space Agency–NASA Cluster Mission or NASA's Magnetospheric MultiScale and Magnetotail Constellation missions scheduled to fly later this decade.

[55] **Acknowledgments.** The authors thank M. Brittnacher and G. Parks for provision of UVI images, keograms, and polar cap area measurements. Also, the contribution of POLAR AKR observations by D. Gurnett and G. Hospodarsky and CANOPUS measurements by G. Rostoker are greatly appreciated. Discussions with J. Birn, V. Angelopoulos, A. Petrukovich, and K. Sigsbee on an earlier version of the paper were also very helpful.

[56] Janet G. Luhmann thanks the referees for their assistance in evaluating this paper.

References

Akasofu, S.-I., The development of the auroral substorm, *Planet. Space Sci.*, *12*, 273, 1964.

Angelopoulos, V., W. Baumjohann, C. F. Kennel, F. V. Coroniti, M. G. Kivelson, R. Pellat, R. J. Walker, H. Luhr, and G. Paschmann, Bursty bulk flows in the inner central plasma sheet, *J. Geophys. Res.*, *97*, 4027, 1992.

Angelopoulos, V., C. F. Kennel, F. V. Coronit, R. Pellat, M. G. Kivelson, R. J. Walker, C. T. Russell, W. Buamjohann, W. C. Feldman, and J. T. Gosling, Statistical characteristics of bursty bulk flow, *J. Geophys. Res.*, *99*, 21,257, 1994.

Angelopoulos, V., et al., Multipoint analysis of a bursty bulk flow event on April 11, 1985, *J. Geophys. Res.*, *101*, 4967, 1996.

Atkinson, G., A scenario covering all phases of nightside convection with

the roles of ion drifts and reconnection determined from the observed field-aligned currents, *J. Geophys. Res.*, *105*, 12,975, 2000.

Baker, D. N., T. I. Pulkkinen, V. Angelopoulos, W. Baumjohann, and R. L. McPherron, Neutral line model of substorms: Past results and present view, *J. Geophys. Res.*, *101*(12), 975, 1996.

Baumjohann, W., G. G. Paschmann, and H. Lu, Characteristics of high-speed ion flows in the plasma sheet, *J. Geophys. Res.*, *95*, 3801, 1990.

Baumjohann, W., M. Hesse, S. Kokubun, T. Mukai, T. Nagai, and A. A. Petrukovich, Substorm Dipolarization and recovery, *J. Geophys. Res.*, *104*, 24,995, 1999.

Birn, J., M. Hesse, G. Harendel, W. Buamjohann, and K. Shiokawa, Flow braking and the substorm current wedge, *J. Geopys. Res.*, *104*, 19,895, 1999.

Craven, J. D., and L. A. Frank, Diagnosis of auroral dynamics using global imaging with emphasis on large-scale evolutions, in *Auroral Physics*, edited by C.-I. Meng, M. J. Rycroft, and L. A. Frank, pp. 273–288, Cambridge Univ. Press, New York, 1991.

Daglis, I. A., and W. I. Axford, Fast ionospheric response to enhanced activity in geospace: Ion feeding of the inner magnetotail, *J. Geophys. Res.*, *101*, 5047, 1996.

Dungey, J. W., Interplanetary magnetic field and the auroral zones, *Phys Rev. Lett.*, *6*, 47, 1961.

Erickson, G. M., N. C. Maynard, W. J. Burke, G. R. Wilson, and M. A. Heinemann, Electromagnetics of substorm onsets in the near-geosynchronous plasma sheet, *J. Geophys. Res.*, *105*, 25,265, 2000.

Fairfield, D. H., Multi-point measurements of magnetotail dynamics, *Adv. Space Res.*, *8*(9), 97, 1988.

Fairfield, D. H., et al., Geotail observations of substorm onset in the inner magnetosphere, *J. Geophys. Res.*, *103*, 103, 1998.

Fairfield, D. H., et al., Earthward flow bursts in the inner magnetotail and their relation to auroral brightening, AKR intensifications, geosynchronous particle injections and magnetic activity, *J. Geophys. Res.*, *104*, 355, 1999.

Fillingim, M. O., G. K. Parks, L. J. Chen, M. Brittnacher, G. A. Germany, J. F. Spann, D. Larson, and R. P. Lin, Coincident POLAR/UVI and WIND observations of pseudobreakups, *Geophys Res. Lett.*, *27*, 1379, 2000.

Fujita, S., M. Itonaga, and H. Nakata, Relationship between Pi2 pulsations and the localized Impulsive current associated with current disruption in the magnetosphere, *Earth Planets Space*, *52*, 267, 2000.

Haland, S., F. Soraas, and S. Ullaland, Propagation velocities and dimensions of plasmoid structures in the near-Earth magnetotail, *Geophys. Res. Lett.*, *26*, 3269, 1999a.

Haland, S., et al., Magnetospheric and ionospheric response to a substorm: Geotail HEP-LD and Polar PIXIE observations, *J. Geophys. Res.*, *104*, 28,459, 1999b.

Hesse, M., and J. Birn, On dipolarization and its relation to the substorm current wedge, *J. Geophys. Res.*, *96*(19), 417, 1991.

Hesse, M., J. Birn, D. N. Baker, and J. Slavin, MHD simulations of the transition of magnetic reconnection from closed to open field lines, *J. Geophys. Res.*, *101*, 10,805, 1996.

Hesse, M., K. Schindler, J. Birn, and M. Kuznetsova, The diffusion region in collisionless magnetic reconnection, *Phys. Plasmas*, *6*, 1781, 1999.

Hones, E. W. Jr., Substorm processes in the magnetotail: Comments on "On hot tenuous plasma, fireballs, and boundary layers in the Earth's magnetotail" by L. A. Frank et al., *J. Geophys. Res.*, *82*, 5633, 1977.

Hori, T., K. Maezawa, Y. Saito, and T. Mukai, Average profile of ion flow and convection electric field in the near-Earth plasma sheet, *Geophys. Res. Lett.*, *27*, 1623, 2000.

Ieda, A., S. Machida, T. Mukai, Y. Saito, T. Yamamoto, A. Nishida, T. Terasawa, and S. Kokubun, Statistical analysis on the plasmoid evolution with Geotail observations, *J. Geophys. Res.*, *103*, 4453, 1998.

Ieda, A., D. H. Fairfield, T. Mukai, Y. Saito, S. Kokubun, K. Liou, C.-I. Meng, G. K. Parks, and M. J. Brittnacher, Plasmoid ejection and auroral brightenings, *J. Geophys. Res.*, *105*, 3845, 2000.

Imhof, W. L., et al., The Polar Ionospheric X-ray Imaging Experiment (PIXIE), *Space Sci. Rev.*, *71*, 385, 1995.

Jacquey, C., J. A. Sauvaud, and J. Dandouras, Location and propagation of the magnetotail current disruption during substorm expansion: Analysis and simulation of an ISEE multi-onset event, *Geophys. Res. Lett.*, *18*, 389, 1991.

Jin, S.-P., X.-P. Hu, Q.-G. Zong, S.-Y. Fu, B. Wilken, and J. Buchner, A 2.5 dimensional MHO simulation of multiple-plasmoid-like structures in the coarse of a substorm, *J. Geophys. Res.*, *106*, 29,807, 2001.

Kallio, E. I., T. I. Pulkkinen, H. E. J. Koskinen, A. Viljanen, J. A. Slavin, and K. W. Ogilive, Loading-unloading processes in the nightside ionosphere, *Geophys. Res. Lett.*, *27*, 1627, 2000.

Kamide, Y., and S. Kokubun, Two-component auroral electrojet: Importance for substorm studies, *J. Geophys. Res.*, *101*, 13,027, 1996.

Kepko, L., and M. Kivelson, Generation of Pi2 pulsations by bursty bulk flows, *J. Geophys. Res.*, *86*, 25,021, 1999.

Kepko, L., M. G. Kivelson, and K. Yumoto, Flow bursts, braking and Pi2 pulsations, *J. Geophys. Res.*, *106*, 1903, 2001.

Kokubun, S., and R. L. McPherron, Substorm signatures at synchronous altitude, *J. Geophys. Res.*, *86*, 11,265, 1981.

Kuznetsova, M., and M. Hesse, Towards a transport model of collisionless magnetic reconnection, *J. Geophys. Res.*, *105*, 7601, 2000.

Lennartsson, W., and E. G. Shelley, Survey of 0.1–16 keV/e plasma sheet ion composition, *J. Geophys. Res.*, *91*, 3061, 1986.

Liou, K., C.-I. Meng, A. T. Y. Lui, P. T. Newell, M. Brittnacher, G. Parks, G. D. Reeves, R. R. Anderson, and K. Yumoto, On the relative timing in substorm onset signatures, *J. Geophys. Res.*, *104*, 22,807, 1999.

Liou, K., C.-I. Meng, P. T. Newell, K. Takahashi, S.-I. Ohtani, A. T. Y. Lui, M. Brittnacher, and G. Parks, Evaluation of low-latitude Pi2 pulsations as indicators of substorm onset using Polar ultraviolet imagery, *J. Geophys. Res.*, *105*, 2495, 2000a.

Liou, K., C.-I. Meng, A. T. Y. Lui, P. T. Newell, and R. R. Anderson, Auroral kilometric adiation at substorm onset, *J. Geophys. Res.*, *105*, 25,325, 2000b.

Lui, A. T. Y., Current disruption in the Earth's magnetosphere: Observations and models, *J. Geophys. Res.*, *101*, 13,067, 1996.

Lyon, J. G., R. E. Lopez, C. C. Goodrich, M. Wiltberger, and K. Papadopoulos, Simulation of the March 9, 1995, substorm: Auroral brightening and the onset of lobe reconnection, *Geophys. Res. Lett.*, *25*, 3039, 1998.

Machida, S., Y. Miyashita, A. Ieda, A. Nishida, T. Mukai, Y. Saito, and S. Kokubun, Geotail observations of flow velocity and north-south magnetic field variations in the near and distant tail associated with substorm onsets, *Geophys. Res. Lett.*, *26*, 635, 1999.

Machida, S., A. Ieda, T. Mukai, Y. Saito, and A. Nishida, Statistical visualization of the Earth's magnetotail during substorms by means of multidimensional superposed epoch analysis with Geotail data, *J. Geophys. Res.*, *105*, 25,291, 2000.

McPherron, R. L., Physical processes producing substorm and storms, *Geomagnetism*, vol. 4, edited by J. A. Jacobs, p. 593, Academic, San Diego, Califor., 1991.

McPherron, R. L., and R. H. Manka, Dynamics of the 1054 UT, March 22, 1979 substorm, *J. Geophys. Res.*, *90*, 1175, 1985.

McPherron, R. L., C. T. Russell, and M. P. Aubry, Satellite studies of magnetospheric substorms on August 15, 1968, 9, Phenomenological model for substorms, *J. Geophys. Res.*, *78*, 3131, 1973.

Miyashita, Y., S. Machida, T. Mukai, Y. Saito, K. Tsuruda, H. Hayakawa, and P. R. Sutcliffe, A statistical study of variations in the near and mid-distant magnetotail associated with substorm onsets: Geotail observations, *J. Geophys. Res.*, *105*, 15,913, 2000.

Moldwin, M. B., and W. J. Hughes, Multi-satellite observations of plasmoids: IMP 8 and ISEE 3, *Geophys. Res. Lett.*, *19*, 1081, 1992.

Moldwin, M. B., and W. J. Hughes, Geomagnetic substorm association of plasmoids, *J. Geophys. Res.*, *98*, 81, 1993.

Moore, T. E., D. L. Gallagher, J. L. Horowitz, and R. H. Comfort, MHD wave breaking in the outer plasmasphere, *Geophys. Res. Lett.*, *14*, 1007, 1987.

Mukai, T., S. Machida, Y. Saito, M. Hirahara, T. Terasawa, N. Kaya, T. Obara, M. Ejiri, and A. Nishida, Low energy particle (LEP) experiment onboard the Geotail onboard the Geotail satellite, *J. Geomagn. Geoelectr.*, *46*, 669, 1994.

Nagai, T., Observed magnetic substorm signatures at synchronous altitude, *J. Geophys. Res.*, *87*, 4405, 1982.

Nagai, T., et al., Initial Geotail survey of magnetic substorm signatures in the magnetotail, *Geophys. Res. Lett.*, *21*, 2991, 1994.

Nagai, T., M. Fujimoto, Y. Saito, S. Machida, T. Terasawa, R. Nakamura, T. Yamamoto, T. Mukai, A. Nishida, and S. Kokubun, Structure and dynamics of magnetic reconnection for substorm onsets with Geotail observations, *J. Geophys. Res.*, *103*, 4419, 1998.

Nagai, T., H. J. Singer, T. Mukai, T. Yamamoto, and S. Kokubun, Development of substorms in the near-Earth tail, *Adv. Space Res.*, *25*(7/8), 1651, 2000.

Ogino, T., and R. J. Walker, Response of the magnetosphere to a southward turning of the IMF: Energy flow and near Earth tail dynamics, in *Substorm*, vol. 4, edited by S. Kokubun and Y. Kamide, p. 635, Kluwer Acad., Norwell, Mass., 1998.

Ohtani, S., F. Creutzberg, T. Mukai, H. Singer, A. T. Y. Lui, M. Nakamura, P. Prikryl, K. Yumoto, and G. Rostoker, Substorm onset timing: The December 31, 1995 event, *J. Geophys. Res.*, *104*, 22,713, 1999.

Perreault, P. D., and S.-I. Akasofu, A study of geomagnetic storms, *Geophys. J. R. Astron. Soc.*, *54*, 547, 1978.

Petrukovich, A. A., et al., Two spacecraft observations of a reconnection pulse during an auroral breakup, *J. Geophys. Res.*, *103*, 47, 1998.

Raeder, J., R. L. McPherron, L. A. Frank, W. R. Patterson, J. B. Sigworth, G. Lu, H. J. Singer, S. Kokubun, T. Mukai, and J. A. Slavin, GLobal simulation of the Geospace Environment Modeling substorm challenge event, *J. Geophys. Res.*, *106*, 381, 2000.

Richardson, I. G., et al., Plasmoid-associated energetic ion bursts in the deep geomagnetic tail: Properties of plasmoids and the post-plasmoid plasma sheet, *J. Geophys. Res.*, *92*, 9997, 1987.

Rostoker, G., Phenomenology and physics of magnetospheric substorms, *J. Geophys. Res.*, *101*(12), 955, 1996.

Russell, C. T., M. Ginsky, and S. M. Petrinec, Sudden impulses at low-latitude stations: Steady state response for southward IMF, *J. Geophys. Res.*, *99*, 13,403, 1994.

Sergeev, V. A., et al., Multiple-spacecraft observations of a narrow transient plasma jet in the Earth's plasma sheet, *Geophys. Res. Lett.*, *27*, 851, 2000.

Shay, M. A., J. F. Drake, R. E. Denton, and D. Biskamp, Structure of the dissipation region during collisionless reconnection, *J. Geophys. Res.*, *103*, 9165, 1998.

Shiokawa, K., W. Baumjohann, and G. Haerendel, Braking of high-speed flows in the near-earth tail, *Geophys. Res. Lett.*, *24*, 1179, 1997.

Shiokawa, K., et al., High-speed ion flow substorm current wedge formation and multiple Pi2 pulsations, *J. Geophys. Res.*, *103*, 4491, 1998a.

Shiokawa, K., G. Haerendel, and W. Baumjohann, Azimuthal pressure gradient as the Driving force of substorm currents, *Geophys. Res. Lett.*, *25*, 959, 1998b.

Singer, H. J., et al., Magnetic disturbances in the vicinity of synchronous orbit and the substorm current wedge: A case study, *J. Geophys. Res.*, *90*, 9583, 1985.

Slavin, J. A., B. T. Tsurutani, E. J. Smith, D. E. Jones, and D. G. Sibeck, Average configuration of the distant magnetotail: Initial ISEE-3 magnetic field results, *Geophys. Res. Lett.*, *10*, 973, 1983.

Slavin, J. A., et al., An ISEE 3 study of average and substorm conditions in the distant magnetotail, *J. Geophys. Res.*, *90*, 10,875, 1985.

Slavin, J. A., M. F. Smith, E. L. Mazur, D. N. Baker, T. Iyemori, H. J. Singer, and E. W. Greenstadt, ISEE 3 plasmoid and TCR observations during an extended interval of substorm activity, *Geophys. Res. Lett.*, *19*, 825, 1992.

Slavin, J. A., M. F. Smith, E. L. Mazur, D. N. Baker, T. Iyemori, and E. W. Greenstadt, ISEE 3 observations of traveling compression regions in the Earth's magnetotail, *J. Geophys. Res.*, *98*, 15,425, 1993.

Slavin, J. A., et al., WIND, GEOTAIL and GOES 9 observations of magnetic field dipolarization and bursty bulk flows in the near-tail, *Geophys. Res. Lett.*, *24*, 971, 1997.

Slavin, J. A., et al., Dual spacecraft observations of lobe magnetic field perturbations before, during, and after plasmoid release, *Geophys. Res. Lett.*, *26*, 2897, 1999.

Taguchi, S., J. A. Slavin, and R. P. Lepping, IMP 8 observations of traveling compression regions in the mid-tail near substorm expansion phase onset, *Geophys. Res. Lett.*, *24*, 353, 1997.

Taguchi, S., J. A. Slavin, M. Kiyohara, M. Nose, R. P. Lepping, and G. Reeves, Temporal relationship between mid-tail TCR and substorm onset: Evidence for NENL formation in the late growth phase, *J. Geophys. Res.*, *103*, 26,607, 1998.

Torr, M. R., et al., A far ultraviolet imager for the ISTP Mission, *Space Sci. Rev.*, *71*, 329, 1995.

Tu, J.-N., K. Tsuruda, H. Hayakawa, A. Matsuoka, T. Mukai, I. Nagano, and S. Yagitani, Statistical nature of impulsive electric fields associated with fast ion flow in the near-Earth plasma sheet, *J. Geophys. Res.*, *105*, 18,901, 2000.

Weiss, L. A., P. H. Reiff, J. J. Moses, R. A. Heelis, and B. D. Moore, Energy dissipation in substorms, in *Substorm 1, ESA SP-335*, Eur. Space Agency, Paris, June 1992.

D. H. Fairfield, M. Hesse, A. Ieda, R. P. Lepping, and J. A. Slavin, Laboratory for Extraterrestrial Physics, NASA/GSFC, Greenbelt, MD 20771, USA. (james.a.slavin@gsfc.nasa.gov)

T. Mukai, Institute of Space and Astronautical Science, 3-1-1 Yoshinodai, Sagamihara, Kanagawa 229, Japan.

T. Nagai, Department of Earth and Planetary Sciences, Tokyo Institute of Technology, 2-12-1 Ookayama, Meguro, Tokyo 152-8551, Japan.

N. Østgaard, Space Sciences Laboratory, University of California, Berkeley, CA 94720-7450, USA.

H. J. Singer, NOAA Space Environment Center, Boulder, CO 80303, USA.

P. R. Sutcliffe, Hermanus Magnetic Observatory, P. O. Box 32, Hermanus 7200, South Africa.

E. Tanskanen, Geophysics Division, Finnish Meteorological Institute, Helsinki FIN-00101, Finland.

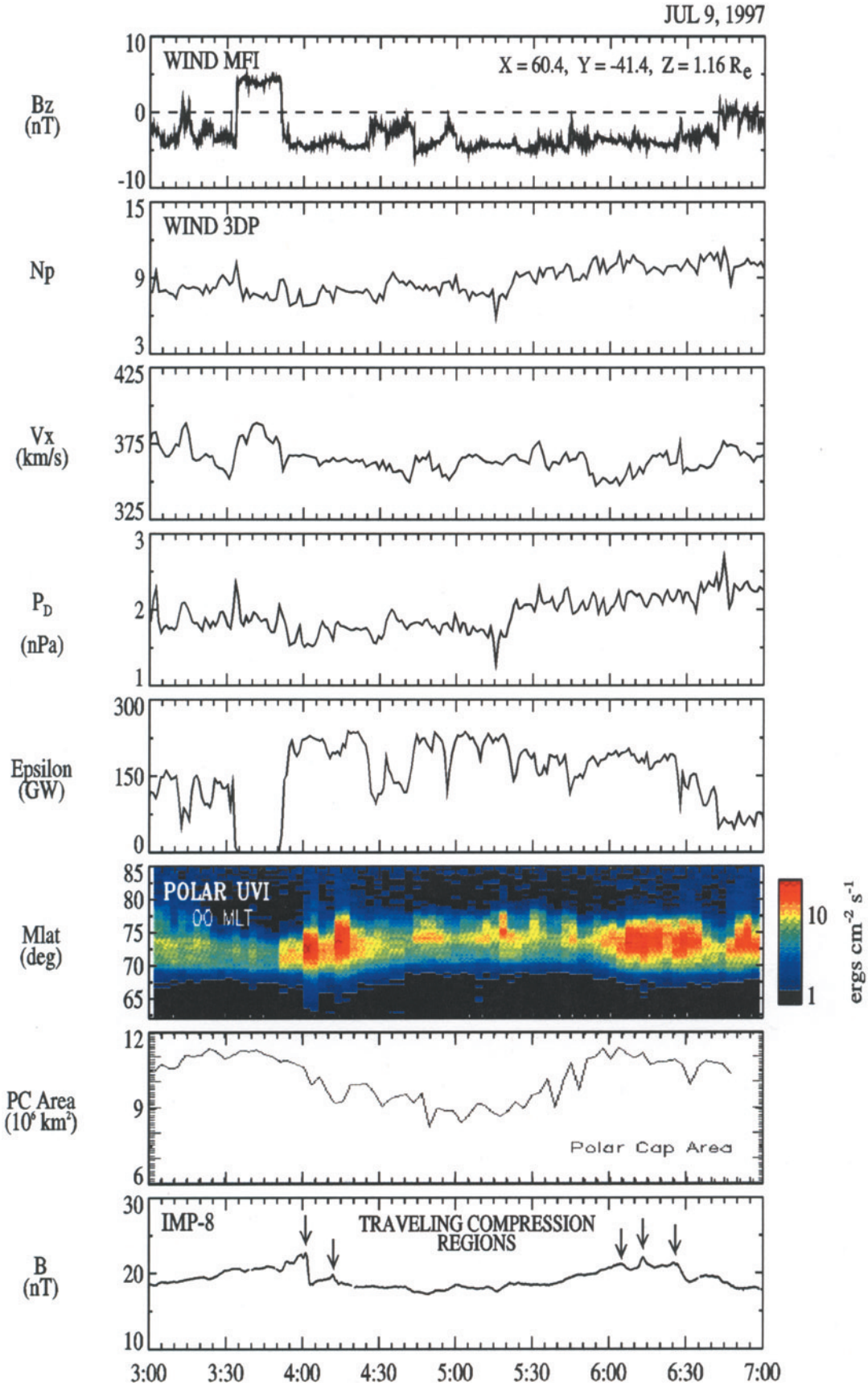

Figure 2. Solar wind and interplanetary magnetic field measurements upstream of the magnetosphere. A midnight sector auroral keogram and polar cap area from the Polar satellite and a plot of the lobe magnetic field intensity at IMP 8. The traveling compression regions are indicated with arrows.

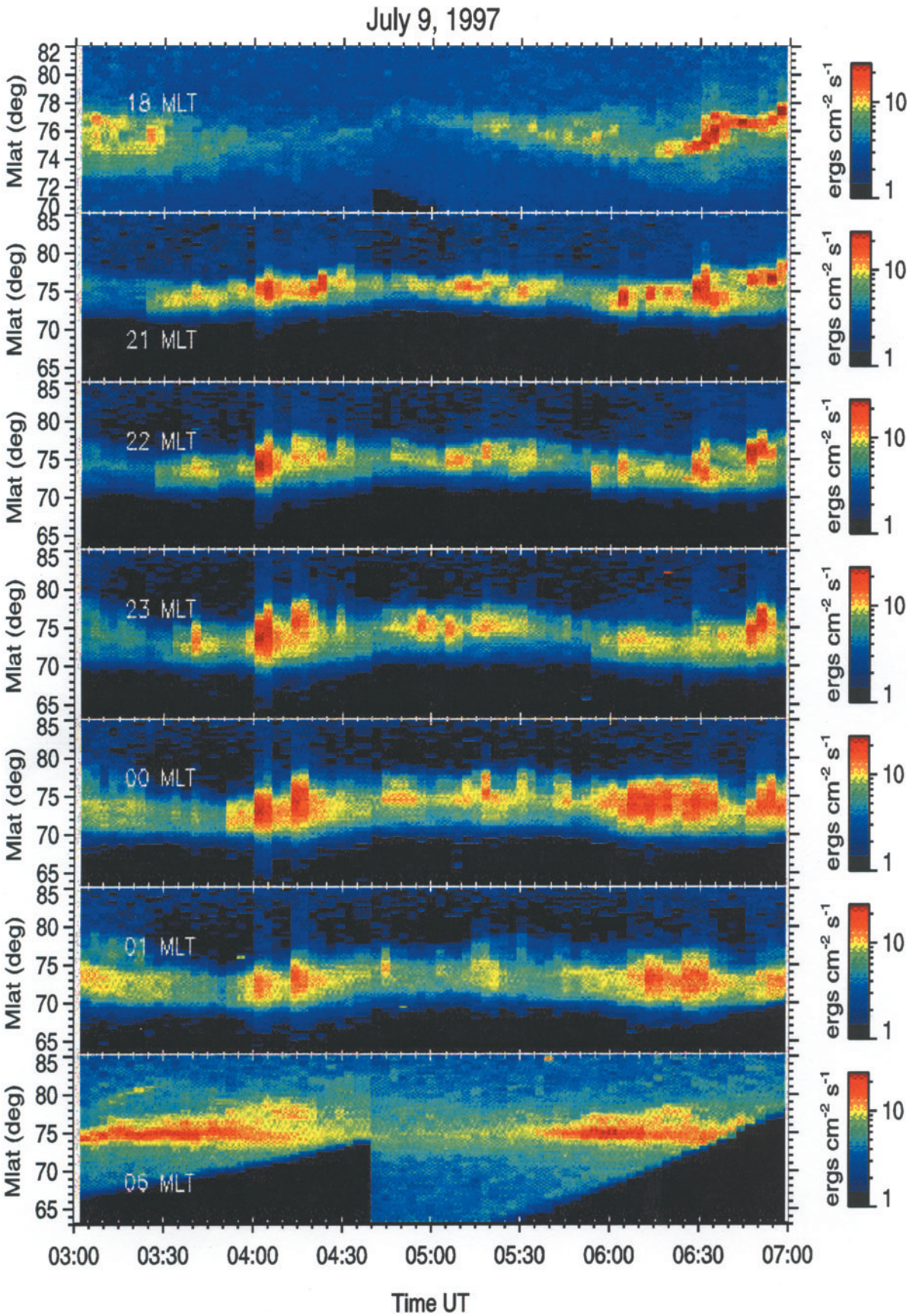

Figure 3. Auroral keograms (i.e., intensity as a function of latitude and universal time) with a spatial resolution of 1 hour in local time and 3 min in universal time.

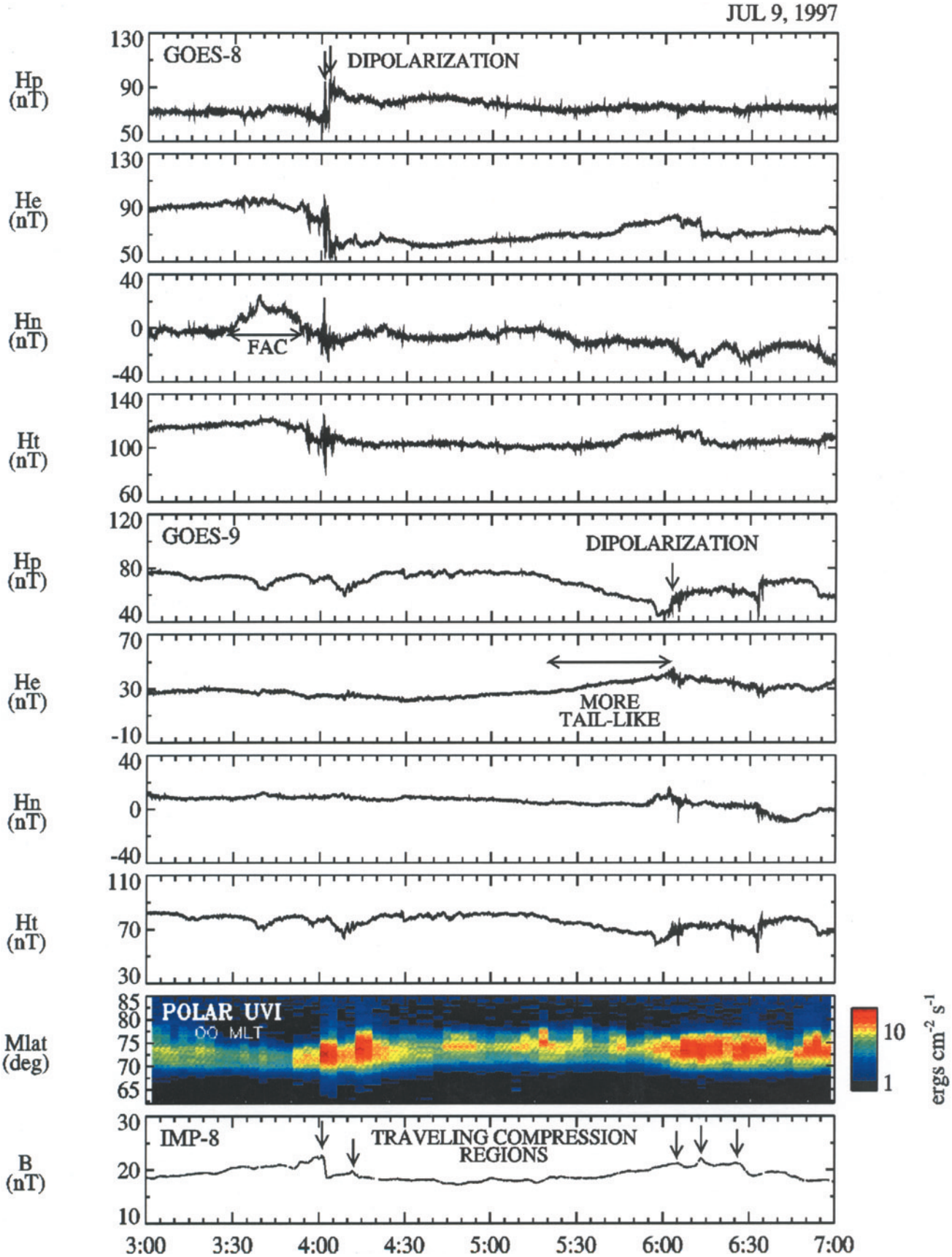

Figure 4. GOES 8 and 9 magnetic field observations in the coordinate system where H_p is parallel and opposite to the geomagnetic dipole, H_e is orthogonal to H_p and positive outward from the Earth, and H_n in positive eastward and completes the right-handed system.

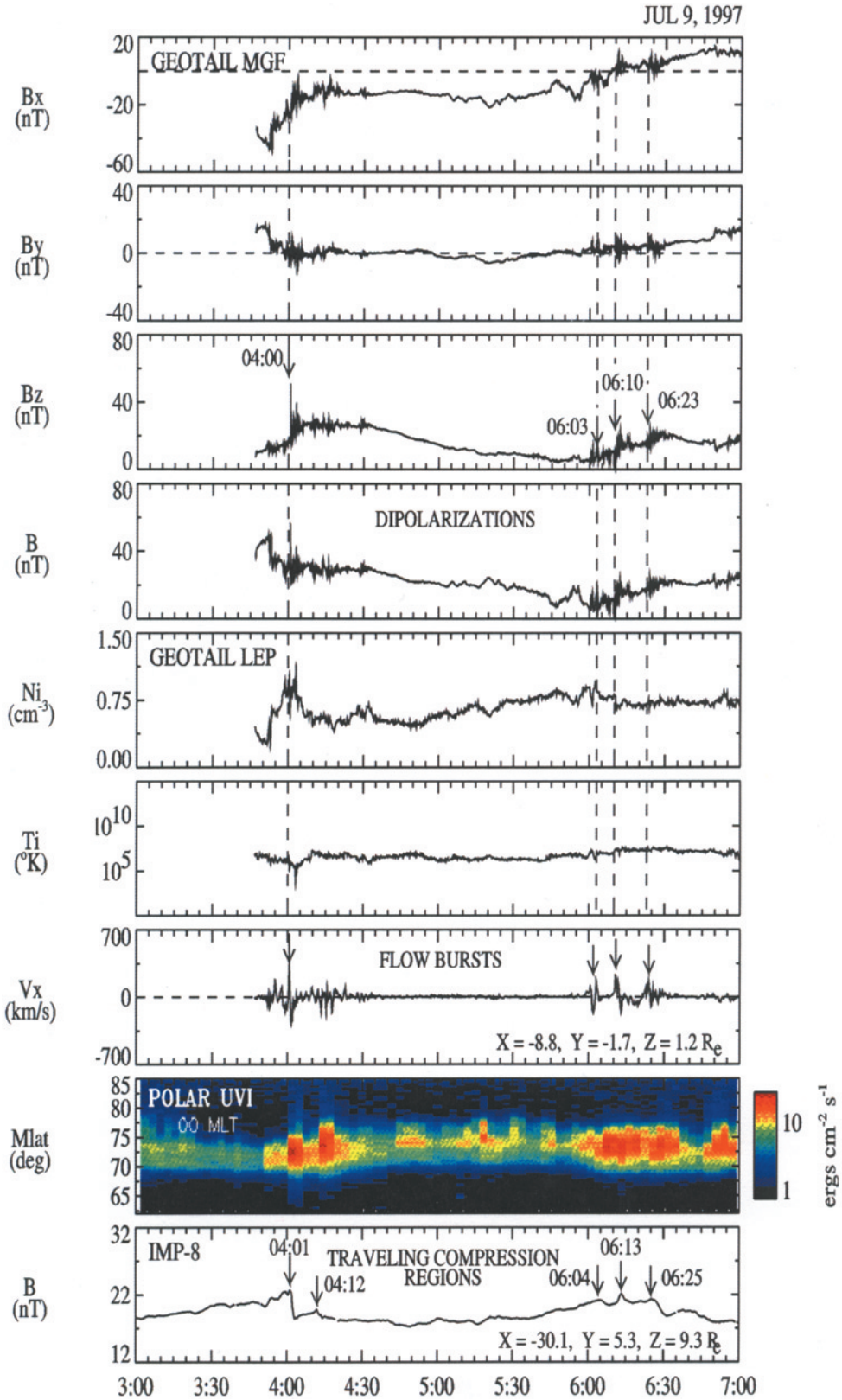

Figure 5. Geotail magnetic field and X component of the plasma flow velocity are displayed in the GSM coordinate system along with ion density and temperature. Vertical dashed lines indicate the times of clear magnetic field dipolarization and plasma flow burst events. Note the close correlation between the dipolarization and flow bursts at Geotail at $X \sim -9\ R_E$ and the TCRs, indicating plasmoid ejection in the IMP 8 magnetic field measurements at $X \sim -30\ R_E$.

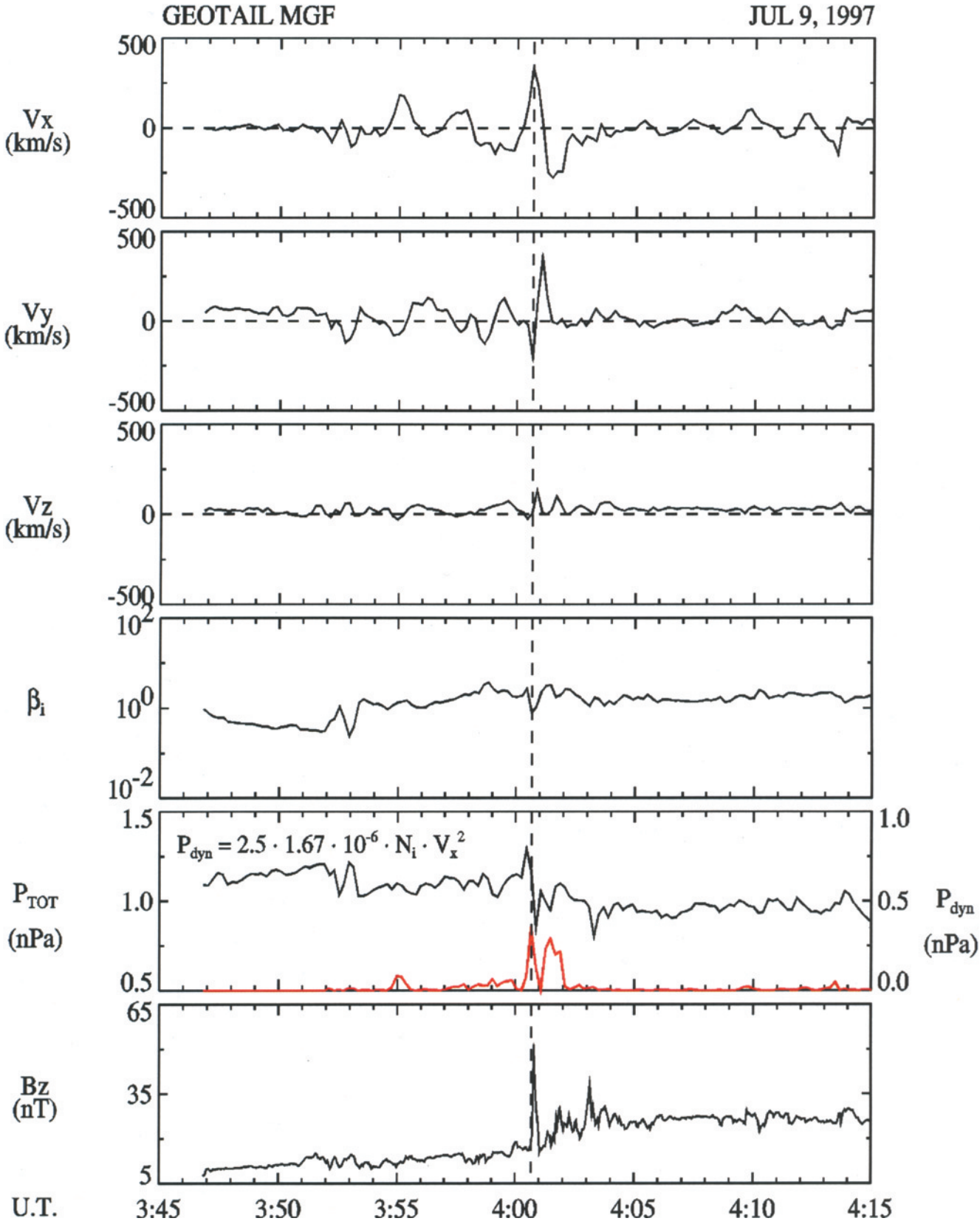

Figure 6. The plasma flow velocity, the plasma ion beta, the total and ram pressures, and the B_z component of the magnetic field are displayed for the first of the substorms under examination. (Note, a plasma sheet composition of 10% O^+ and 90% H^+ has been assumed in calculating the plasma sheet flow ram pressure.)

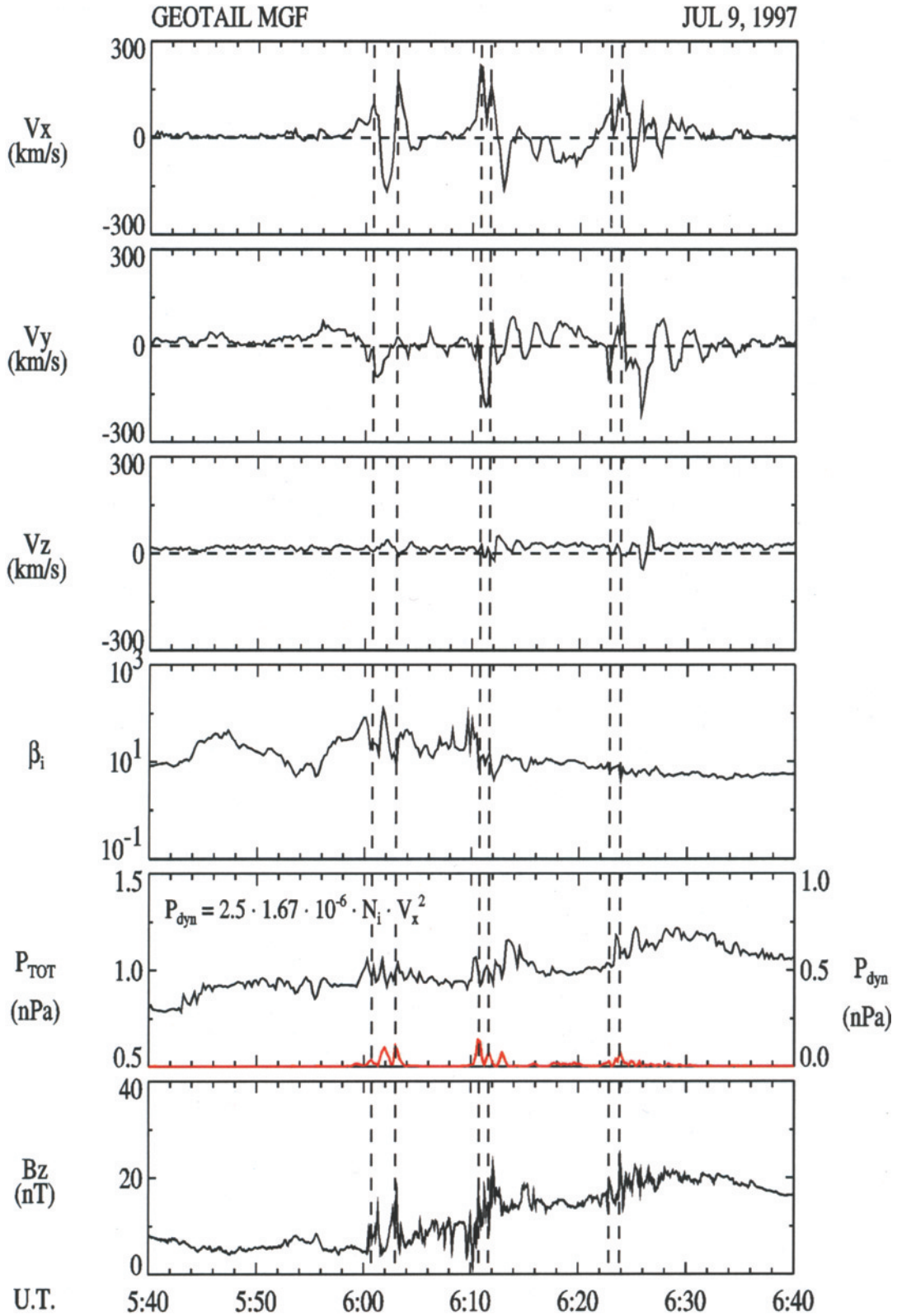

Figure 7. The plasma flow velocity, plasma ion beta, the total and ram pressures, and the B_z magnetic field component are displayed for the second substorm in the same format as in Figure 6. Note the step-like progression of magnetic dipolarization at Geotail.

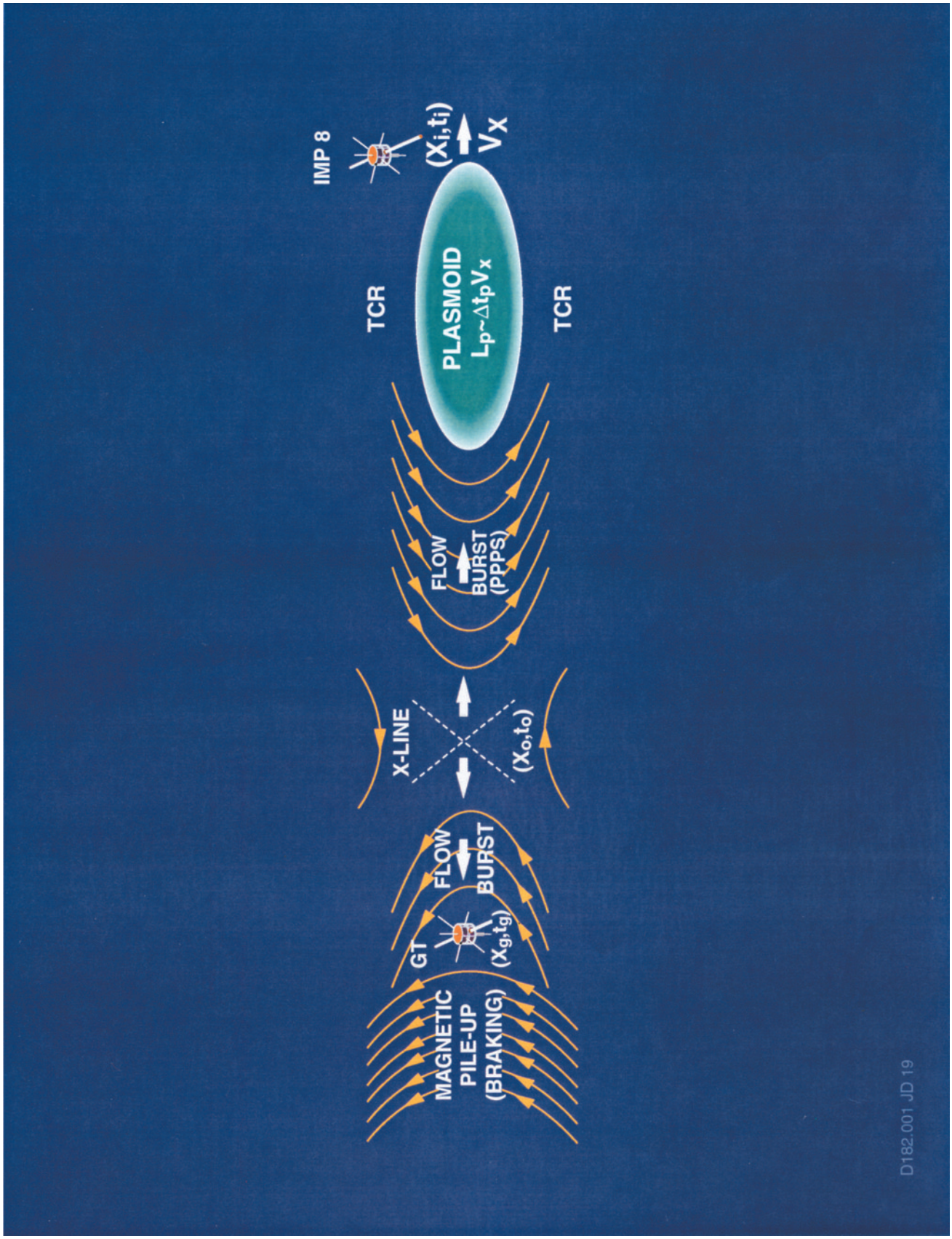
IMP 8
(X_i,t_i)
V_X
TCR
PLASMOID
$L_p \sim \Delta t_p V_x$
TCR
FLOW
BURST
(PPPS)
X-LINE
(X_o,t_o)
FLOW
BURST
GT
(X_g,t_g)
MAGNETIC
PILE-UP
(BRAKING)
D182.001 JD 19

Figure 11. Meridian cut through the central tail showing the earthward and tailward consequences of the onset of open field line reconnection; earthward and tailward high-speed flows, flow braking and dipolarization, and plasmoid ejection.

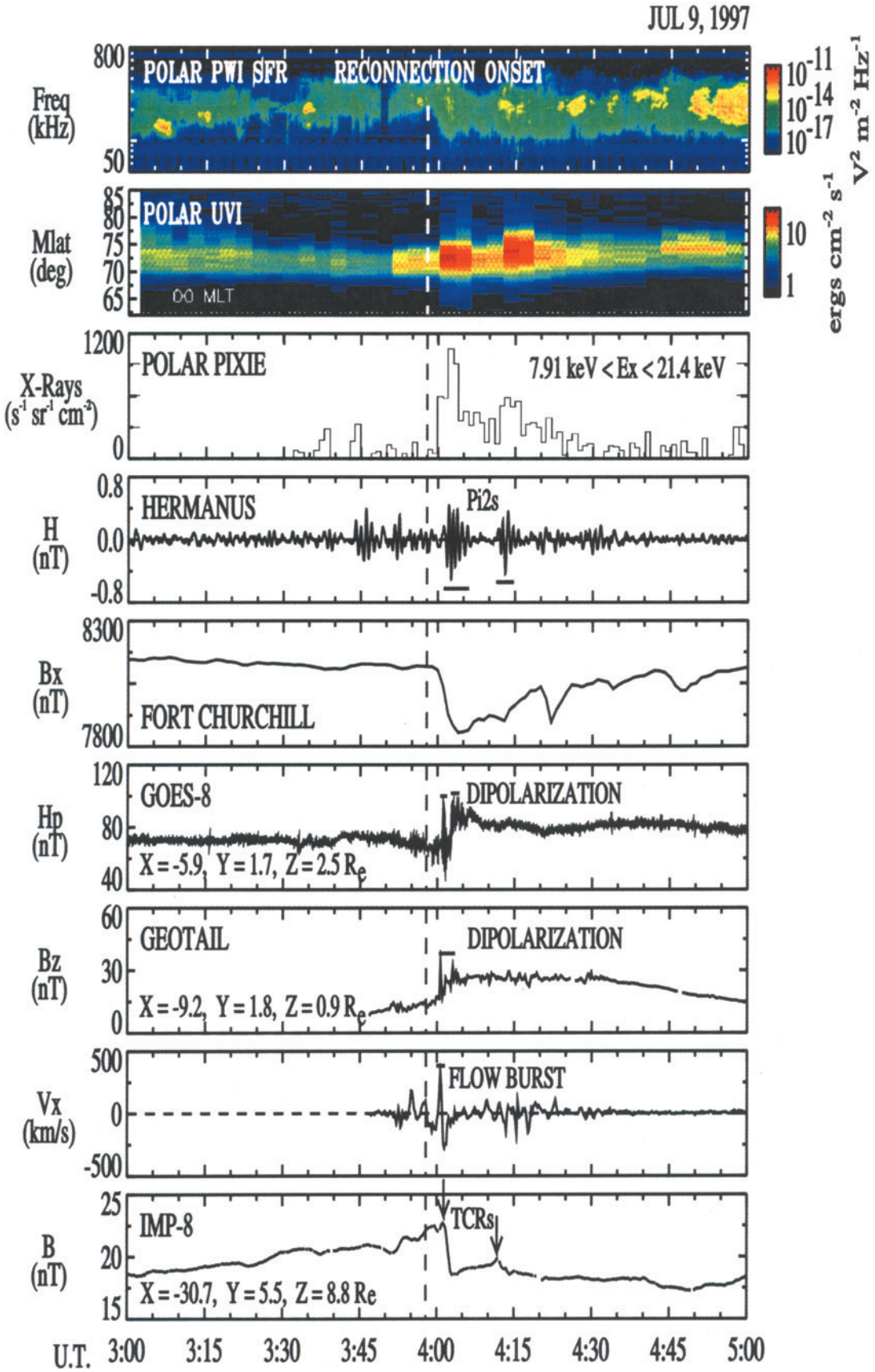

Figure 12. A summary of the ISTP observations for the first substorm is presented with a vertical dashed line marking the inferred time of the onset of lobe field line reconnection at the NENL.

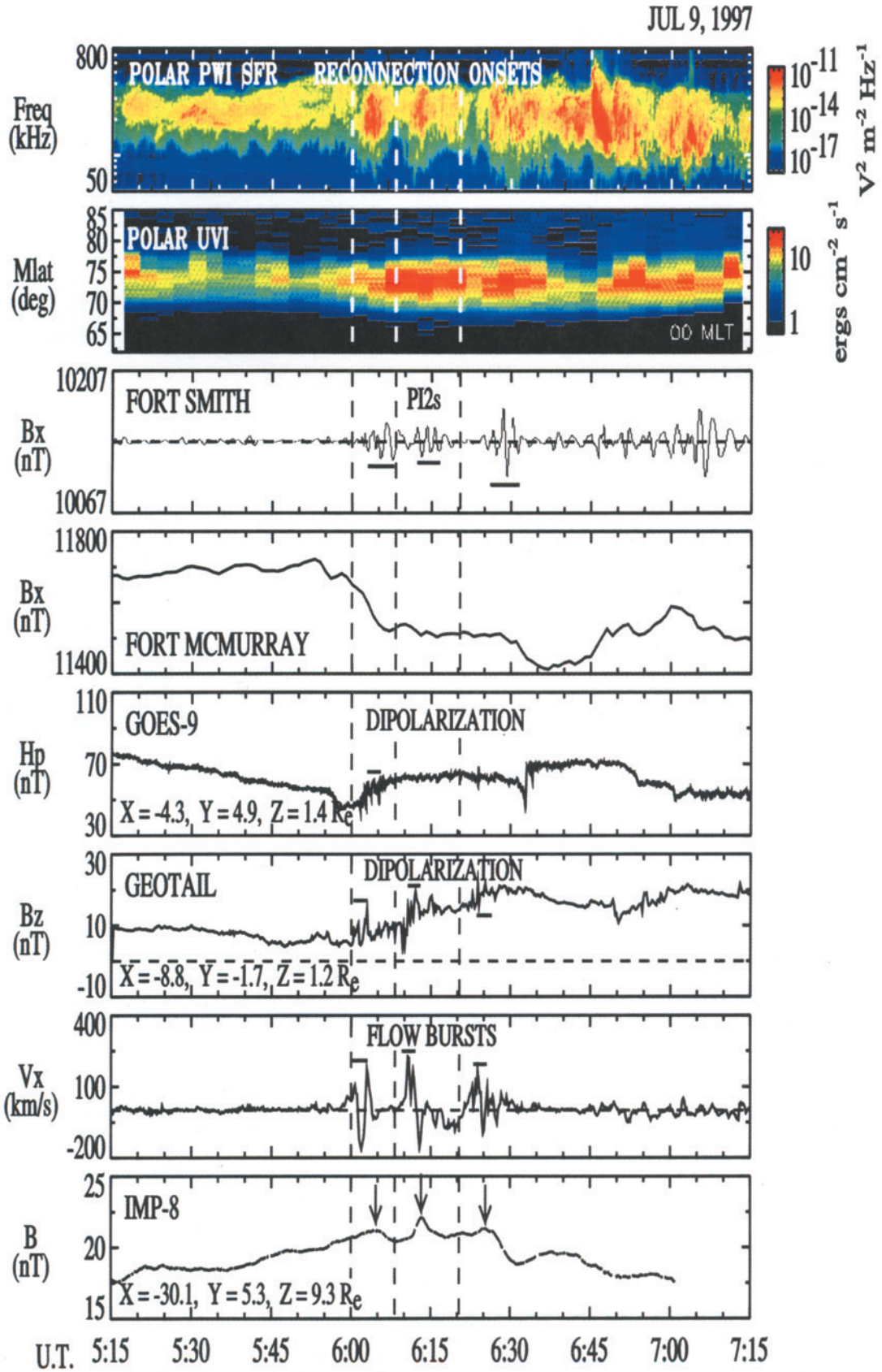

Figure 13. A summary of the ISTP observations for the second substorm is presented with vertical dashed lines marking the inferred times for the onset of lobe field line reconnection at the NENL associated with each episode of earthward flow bursts.